Simultaneous Measurement of Perfusion and T_2* in Calf Muscle at 7T with Dynamic Exercise using Radial Acquisition.

by

Sultan Zaman Mahmud

A thesis submitted to the Graduate Faculty of
Auburn University
in partial fulfillment of the
requirements for the Degree of
Master of Science

Auburn, Alabama
May 4, 2019

Keywords: Perfusion, T_2*, BOLD, MRI, Dynamic Exercise, Radial Imaging.

Approved by

Adil Bashir, Chair, Associate Professor of Electrical and Computer Engineering
Thomas Denney, Professor of Electrical and Computer Engineering
Stanley Reeves, Professor of Electrical and Computer Engineering

Abstract

Impairments in oxygen delivery and consumption can lead to muscle weakness and physical disability. Reduced blood flow, O_2 delivery and consumption to the working muscle are likely to cause decline in muscle ability to sustain workloads. Perfusion is a measure of microvascular blood flow and provides information on nutrients delivery. T_2* provides information about relative tissue oxygenation. Changes in these parameters following stress, such as exercise, can yield important information about imbalance between delivery and consumption. In this study, we implemented a novel MRI projection reconstruction technique to simultaneously quantify muscle perfusion and T_2* at high magnetic field, 7T, and demonstrate assessment of spatial and temporal changes in these parameters within calf muscles both during and recovery from dynamic exercise. The high magnetic field offers significant improvement in the signal to noise ratio and the projection based reconstruction, which uses golden angle radial acquisition, offers very low sensitivity to bulk motion of the subject inside the MRI scanner.

Acknowledgments

I would like to thank my advisor, Dr. Adil Bashir. He is one of the nicest persons I have ever met. Without his guidance and help this journey would not have been so smooth. I would also like to thank other committee members, Dr. Thomas Denney and Dr. Stanley Reeves for their support. Last but not the least, I would like to thank my parents and my brothers. You are the reasons I am still holding on. If it's not a life that begins with you, it's not a life worth living.

Table of Contents

List of Tables

List of Figures

List of Abbreviations

MRI	Magnetic Resonance Imaging
BOLD	Blood Oxygen Level Dependent
MVC	Maximum Voluntary Contraction
PLD	Post Labeling Delay
ASL	Arterial Spin Labeling
PASL	Pulsed Arterial Spin Labeling
SATIR	Saturation Inversion Recovery
GRE	Gradient Recalled Echo
SS	Slice Selective
NS	Non Slice Selective
FOV	Field Of View
TE	Time of Echo
TR	Time of Repetition

Chapter 1

Introduction

Impairments in nutrients delivery such as oxygen can lead to reduced muscle endurance and physical disability. Perfusion is the delivery of arterial blood to the capillary blood in biological tissue [1]. As arterial blood is oxygenated blood, perfusion also provides information about the delivery of oxygen to the tissue. Accurate quantification of perfusion provides valuable information about muscle metabolism and is an active area of research [2]. It is especially important in the organs such as skeletal muscles where physical demand, oxygen delivery and consumption are tightly coupled [3]. Integrated functions of respiratory, muscular and cardiovascular system are reflected in the measurement of perfusion in the muscle. Studies have shown that the dynamics of skeletal muscle perfusion can provide insight into vascular reactivity [4-7]. So characterizing this quantity is very important. Le Bihan proposed one of the early approaches of perfusion weighted MRI. This approach relies on diffusion MRI to estimate blood flow using he principles of Brownian motion and capillary orientation. This approach has been replaced with arterial spin tagging as the primary non-invasive MR method to quantify perfusion in tissue. Arterial spin tagging uses the magnetization of the inflow blood to the tissue as an endogenous tracer. Several important hemodynamic parameters are determined from perfusion MRI such as blood volume (BV), defined as the volume of blood occupied within a voxel, mean transit time (MTT) which describes average time (temporal width) that the blood spends in the

tissue, and blood flow (BF) which is the volume of blood delivered to the tissue per unit volume, per minute [8]. BF is estimated form BV and MTT using "central volume principle":

$$BF = \frac{BV}{MTT}$$

Oxygen consumption in the muscle is required for energy production and physical work. An estimate of the oxygen content in the tissue can be determined from T_2* relaxation time constant. T_2* signal decay has contributions from inherent "true" T_2 of the tissue and signal dephasing due to magnetic field inhomogeneities:

$$\frac{1}{T_2^*} = \frac{1}{T_2} + \gamma \Delta B_i$$

where ΔB_i is the magnetic field inhomogeneity and γ is the gyromagnetic ratio.

Magnetic field inhomogeneity affecting T_2* is caused by several factors, such as susceptibility differences between tissue interfaces, accumulation of iron inside the cells, oxygen saturation of blood in small vessels and presence of metallic objects. T_2* in general can lead to artifacts in images such as image distortion near tissue – air interfaces or near metallic implants such as dental implants. However, it can be exploited for useful clinical applications; such as pathological levels of iron accumulation in brain and liver [9], imaging of hemorrhages due to paramagnetic contrast [10, 11], susceptibility weighted imaging e.g. MR venography [12].

Quantification of muscle perfusion provides information about oxygen supply to muscular tissues. Local change in blood flow affects blood oxygen level dependent (BOLD) signal. T_2* provides information about total amount of deoxyhemoglobin in the tissue. This is associated with the oxygen saturation in the tissue, which is an indirect measurement of oxygen extraction by the tissue. Oxygen consumption is a key factor behind muscle metabolism and functional abnormality. BOLD signal is also observed as a change of T_2*. So monitoring the blood flow and oxygen consumption, which is related to T_2*, simultaneously can provide information about oxidative metabolism in skeletal muscle. Reduced muscle endurance is the main cause behind muscle disability. So combined measurement of dynamic perfusion and T_2* in organs such as skeletal muscle, where oxygen supply and consumption are tightly coupled, can provide important information about functional deficits in a situation of increased blood flow demand similar to exercise and cardiac stress. This is the main motivation of our current study.

Chapter 2

Available Methods

2.1 Perfusion

Three major types of perfusion MRI techniques are the Dynamic Susceptibility Contrast (DSC), Dynamic Contrast-Enhanced (DCE), and Arterial Spin Labeling (ASL) methods.

2.1.1 Dynamic Susceptibility Contrast (DSC) MRI

This approach relies on magnetic field inhomogeneity created by passage of bolus of MR contrast agent, typically Gadolinium based chelate, through the tissue. As the contrast agent passes through, the vessels become more paramagnetic and create magnetic field inhomogeneities around the vessels. This causes a decrease in the T_2* in the tissue and rapid imaging techniques are used to generate T_2* weighted images. With rapid dynamic imaging it is possible to measure the passage of contrast agent through the tissue and complex mathematical models are used to generate BF, BV. The mathematical models require measurement or knowledge of the arterial input function (AIF) and a deconvolution with AIF is required to calculate BF and BV maps. Partial volume effects hampers accurate measurement of the arterial input function. Another disadvantage of this approach is that it requires injection of exogenous contrast agent [13].

2.1.2 Dynamic Contrast-Enhanced (DCE) MRI

DCE is also an invasive technique and requires external contrast agent. The paramagnetic contrast agent has concentration dependent effect on the longitudinal relaxation time (T_1 relaxation time). As the hemodynamic signal of DCE MRI depends on the value of T_1, shortening of T_1 value increases the DCE signal [14]. Acquisition of rapid T_1-weighted images is used to quantify the change in the signal in the tissue caused by the contrast agents. Permeability of the capillaries, their surface area and perfusion determine the rate at which the contrast agents diffuse from the extracellular blood into the tissue extracellular space.

2.1.3 Arterial Spin Labeling (ASL)

Arterial spin labeling allows for non-invasive quantification of perfusion in the tissues. In this approach the incoming blood spins are magnetically labeled which then act as diffusible tracer when it reaches the tissue [15]. ASL does not use any contrast agent or ionizing radiation and is completely non-invasive technique. The non-invasive nature makes it ideal for repeated measurements in human studies. In ASL technique, two images are acquired to quantify perfusion: one with magnetic labeling of the incoming blood and the other without labeling of the blood. A difference of these two images is used to determine the blood entering the tissue and calculate perfusion maps. Time delay is required for the labeled blood to enter the tissue and is used with other physiological parameters to calculate the perfusion.

As ASL method does not require any contrast agent, therefore it is more convenient and easier to use. As mentioned above, this technique uses subtraction of two images: one with the magnetic tagging of the blood (tag image) and the other without tagging of the blood (control image). For the tag image, water protons in the blood are tagged at the level of large feeding arteries. This

tagged blood spin then flows into the imaging slice and start exchanging with the tissue. At this time, the tag image is acquired, which reflects the signal from both tissue and incoming blood. In the case of control image, blood is not tagged and the signal is only from the tissue. The difference of these two image is proportional to the blood that is delivered to that tissue. This difference images is used to calculate the absolute value of perfusion.

There are three major of labeling techniques used in ASL approach [16]: continuous ASL (CASL), pulsed ASL (PASL), and velocity selective ASL (VSASL). CASL is a steady state approach where the inflowing blood is labeled continuously by a series of RF pulses [17] and temporal resolution is also limited to 6–8 seconds [18,19]. PASL uses a single short radiofrequency pulses to label the blood in a large region that is adjacent to the imaging volume [20]. Since PASL on one RF pulse for labeling it reduces RF energy deposition and allows to measure perfusion at a temporal resolution ~2 seconds [21]. Several different labeling techniques have been successfully demonstrated [22 - 28]. VSASL uses a different approach and labels the blood based on its velocity [29] rather than its spatial location. In this approach the blood flowing below a threshold velocity is labeled and this can avoid transit time problems.

2.2 T_2*

After an RF excitation, the transverse MR signal termed as Free Induction Decay (FID) can be measured. The FID is damped by exponential decay with time constant T_2* (Figure 2.1). T_2* decay composes of the true T_2 decay and dispersion of the spins due to the presence of magnetic field inhomogeneities. A gradient echo (GRE) pulse sequence is typically used to generate T_2* weighted

MR images [30]. A series of images with different echo times are acquired to generate T_2* maps. The signal intensities of these images are fitted to the following equation generates T_2* maps

$$S(x, y, t) = S(x, y) * e^{-\frac{t}{T_2^*}}$$

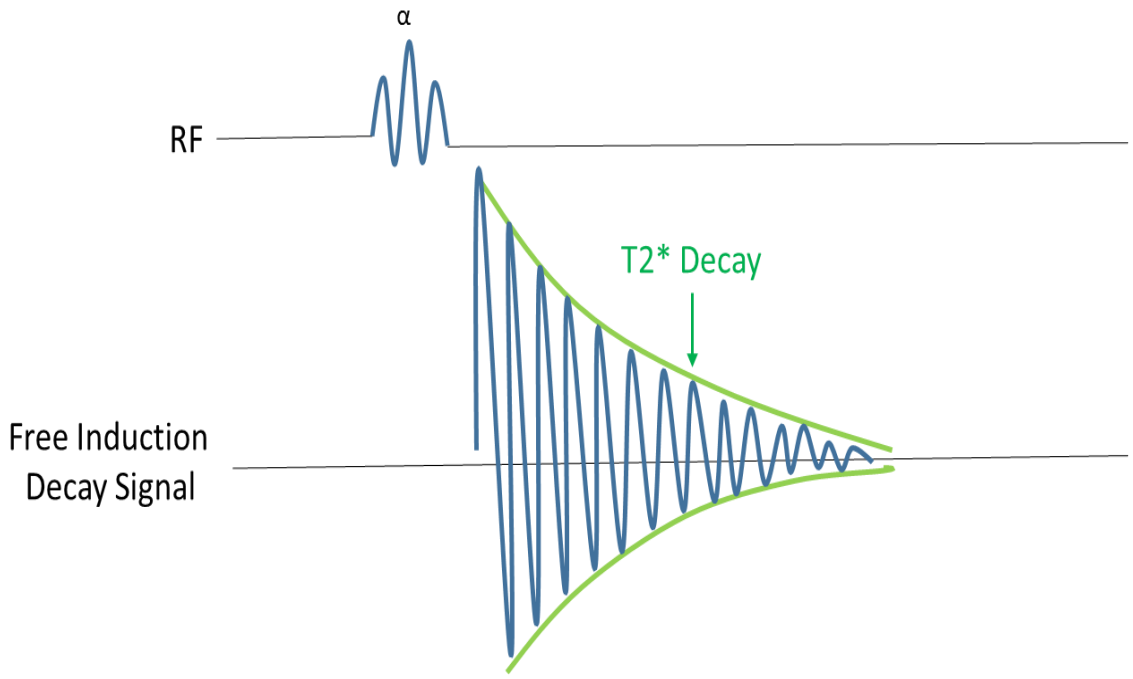

Figure 2.1: T_2* decay

Chapter 3

Theory

PASL is a widely used non-invasive method for perfusion imaging [31-33]. Several variants of PASL techniques have been developed. In this work Saturation Inversion Recovery (SATIR) [34] is used for skeletal muscle perfusion studies. SATIR uses a slice-selective (SS) and non-selective (NS) inversion pulses to acquire tag and control images, respectively. A slice-selective saturation pulse is applied after each acquisition to diphase any residual signal.

3.1 Theory of Saturation Inversion Recovery (SATIR) Imaging of Perfusion

Details of SATIR approach have been described previously and are summarized here [34]. The magnetization properties of the labeled blood entering the tissue is not the same as the magnetization of the tissue therefore a modified Bloch equation is required to describe the signal behavior [35] :

$$\frac{dM(t)}{dt} = f.[M_a(t) - M_v(t)] - r_1.[M(t) - M_o] \quad [1]$$

where $M_v(t)$, $M_a(t)$ and $M(t)$ are magnetization of venous blood, arterial blood and tissue water, respectively. f is the tissue perfusion and r_1 ($r_1 = {}^{1}/_{T_1}$) is the spin-lattice relaxation rate constant of the tissue. Tissue magnetization, M_0, is related to venous, M_v and arterial, M_a, magnetization

through a blood/tissue partition coefficient, λ, given by $M_v = M_a = M_0/\lambda$ at equilibrium. This relationship assumes that there is rapid and full exchange between blood and tissue water.

In classical ASL technique, flow-sensitive alternating inversion-recovery (FAIR) approach f can be calculated by from Eq. [1] from two sets of measurements using slice selective (SS) and nonselective (NS) inversion pulses [36] to prepare each imaging scan, with the result that M_a at t = 0 is also alternately tagged (or "labeled") M_a and $-M_a$ and:

$$\frac{dM_{SS}(t)}{dt} = f.M_a - \frac{f}{\lambda}.M_{SS}(t) - r_1.[M_{SS}(t) - M_o] \quad [2]$$

$$\frac{dM_{NS}(t)}{dt} = f.M_a - \frac{f}{\lambda}.M_{NS}(t) - r_1.[M_{NS}(t) - M_o] \quad [3]$$

Where r_{1a}, the arterial water relaxation rate constant = $1/T_{1a}$ and $M_a(t) = M_a.(1-2\exp(2r_{1a}.t))$. Is the magnetization (M) at the imaging slice is identical prior to SS and NS inversion pulses the perfusion becomes independent of tissue magnetization at t = 0. SATIR approach is based on this philosophy and allows for rapid dynamic imaging of perfusion with temporal resolution on the order of 1 – 2 seconds. Raynaud et al. [34] have shown that under appropriate conditions the perfusion can be readily determined from

$$f = -\frac{\lambda}{T_d}.\ln\left[1 + \frac{M_{SS}(T) - M_{NS}(T)}{M_{SS}(T) + M_{NS}(T)}.\left(1 - e^{\frac{T}{T_1}}\right)\right] \quad [4]$$

where T_d is the arterial labeling delay.

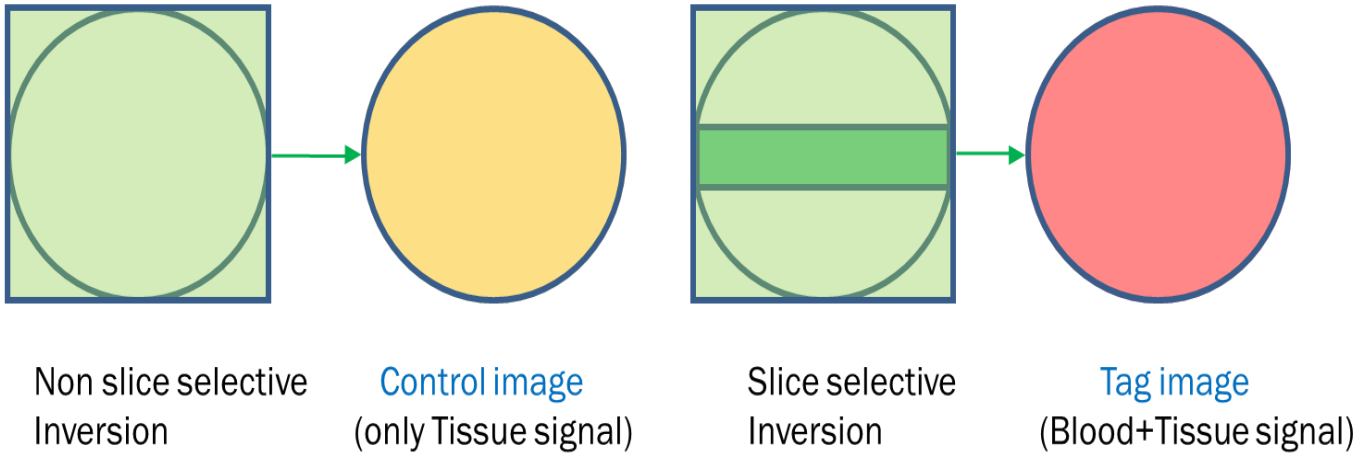

Figure 3.1: Non Slice Selective and Slice Selective acquisition scheme for control and tag image.

3.2 T_2*

Oxygen saturation of the blood affects the local magnetic field homogeneity in the tissue. As cells consume more oxygen the deoxyhemoglobin concentration in the blood increases and it becomes more paramagnetic thus increasing the local magnetic field inhomogeneity. This increase in the local field inhomogeneity causes phase dispersion in transverse magnetization and reduces the apparent transverse relaxation time, T_2*. Hence, change in the value of T_2* represents the level of total deoxyhemoglobin and therefore the level of oxygenation of the tissue. T_2* plays a very important role in blood oxygen level dependent signal (BOLD) signal contrast. A multi echo GRE sequence is used to quantify T_2* as described above.

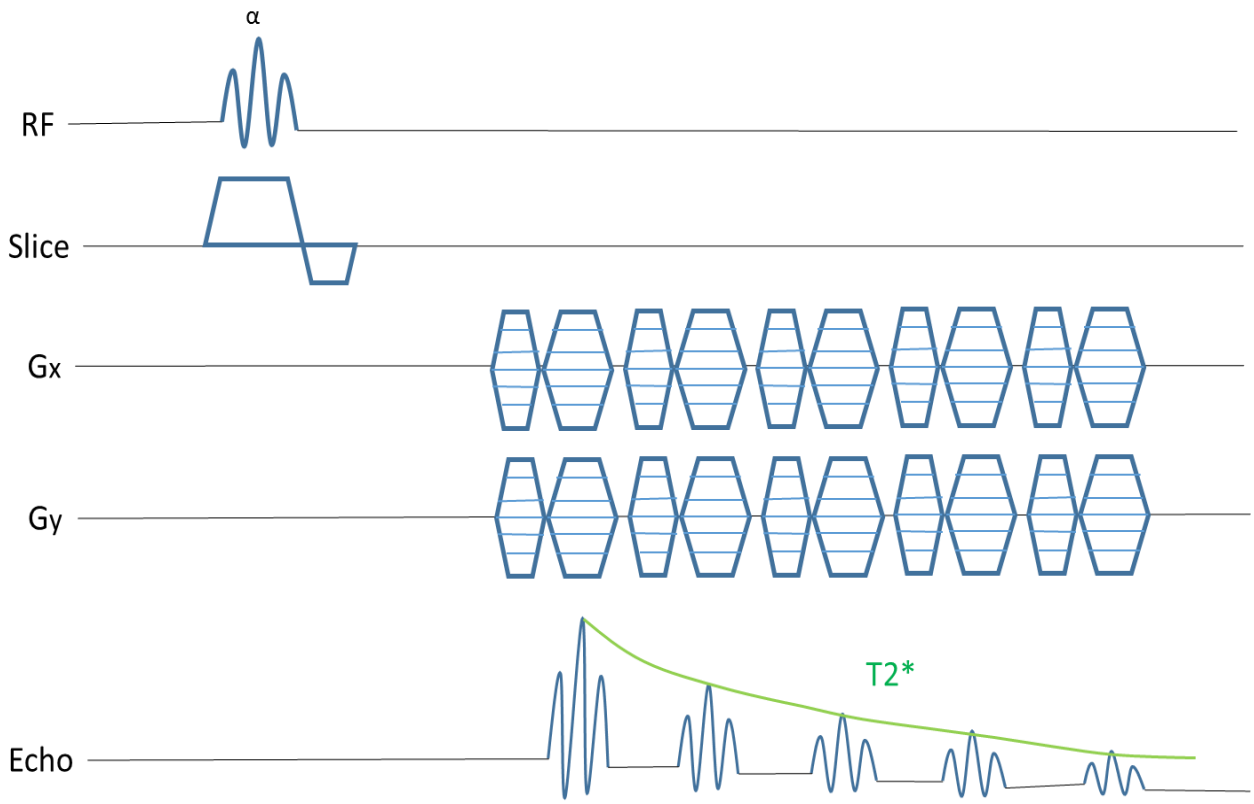

Figure 3.2: Multi echo GRE acquisition for T_2* quantification with radial acquisition.

3.3 Combined Measurement of Perfusion and T_2*

Perfusion measurements require a time delay (T_d) for the magnetically labeled blood to enter the imaging slice. This a dead time between RF pulse use for arterial blood tagging and image acquisition block. This dead time can be used to initiate a multi echo GRE sequence in a distal slice location. The multi echo images acquired from this sequence can be used to calculate the T_2*. This approach enables us to measure perfusion and T_2* in a single scan.

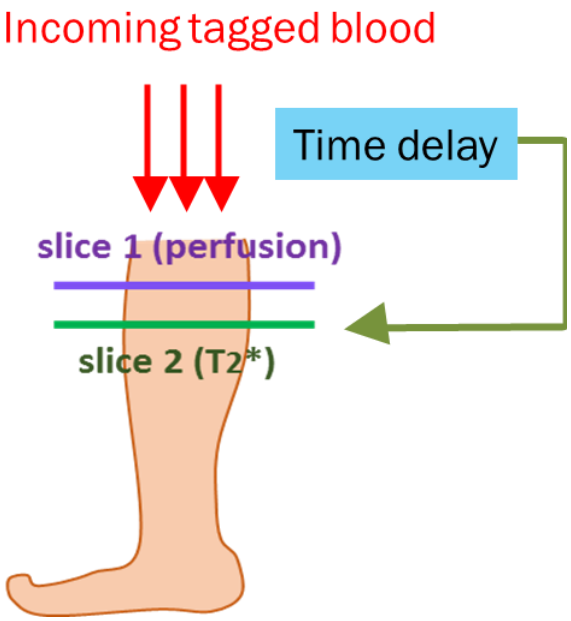

Figure 3.3: Scheme for simultaneous measurement of Perfusion and T_2* in a single scan.

In the time period (T_d) the blood takes to flow into the perfusion slice after slice selective inversion pulse, multi echo T_2* sequence is initiated in another slice 3 cm distal from perfusion slice. After multi echo GRE acquisition control and tag images are acquired in perfusion slice at the end of labeling delay.

Chapter 4

Radial Sampling

In conventional Cartesian MR imaging the data is acquired on a rectangular grid as shown in (Figure 4.1a). In Cartesian sampling all the data points for a given phase encoding line are acquired and then the acquisition moves to the next phase encoding step. Image is reconstructed performing 2D Fourier Transform (2DFT) of the acquired k-space data. Radial imaging is a projection acquisition and reconstruction method similar to computed tomography. In this method, projections at different angles of the target subject, are sampled to fill up the k-space (Figure 4.1b). Since radial sampling takes projections at different angles so the data points do not fall into rectangular Cartesian grid points and 2DFT cannot be used to reconstruct images. Several approaches have been developed to reconstruct images from non-uniform k-space sampling. The most common approach is resampling the radial data to Cartesian grid and then using 2DFT to generate images.

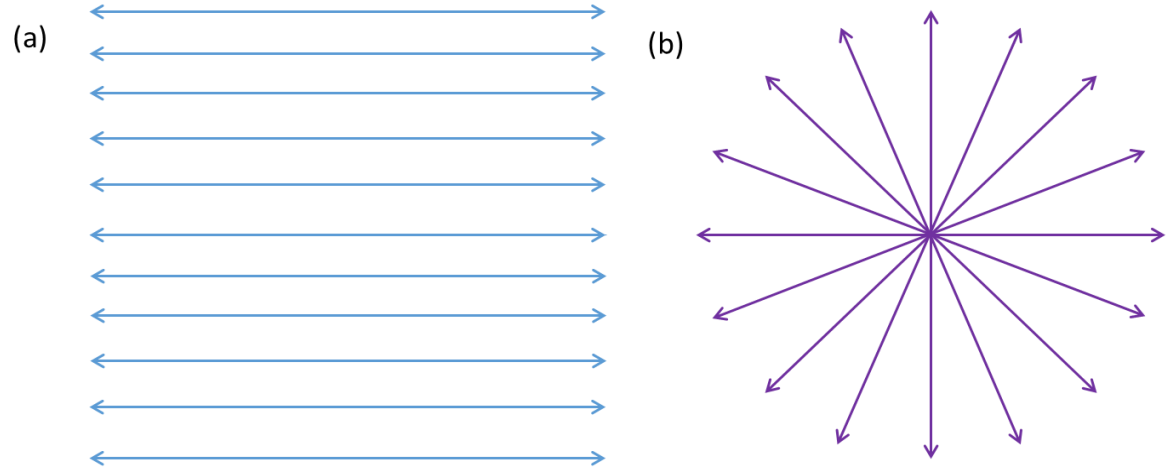

Figure 4.1: Cartesian k-space trajectory (a) and radial k-space trajectory (b).

Gridding to Cartesian k-space points is the first step in reconstructing images from radial acquisition [37]. Gridding involves convolution of the radially acquired samples with appropriate convolution kernel to generate sample point on a Cartesian grid. All Radial data point have a contribution to the nearest Cartesian grid locations. Kaiser-Bessel convolution kernel is the most common kernel used [37]. 2DFT of the resampled k-space is used for reconstruction of images.

There are several advantages of radial sampling

- No phase encoding is used in radial acquisition therefore the method is less sensitive to bulk motion
- Radial acquisition is uniquely suited for under sampled acquisition thus improving temporal resolution for dynamic studies.
- Center of k-space is naturally oversampled hence contrast is preserved even if there is motion in some projections. This also reduces impact of bulk motion.

Radial projections can be acquired in any order, typically projections are either incremented uniformly or using a golden angle acquisition approach [38]. In uniform acquisition, the angle between two successive radial spokes is 360^{o}/total number of radial spokes. In golden angle acquisition, the angle between two successive acquisitions is incremented by 111.25^{o} [39]. This increment divides the largest remaining angular gap between projections in into half for each successive acquisition and results in less artifacts.

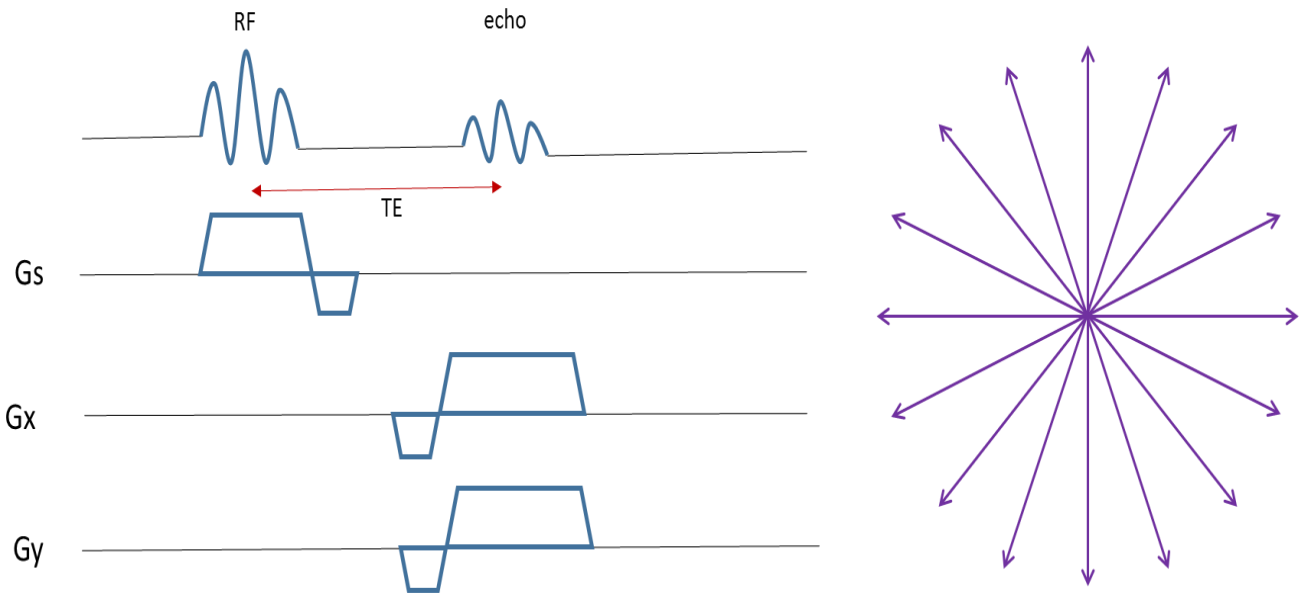

Figure 4.2: Pulse sequence for radial acquisition.

Chapter 5

Related work

While methods for simultaneous quantification of perfusion and T_2* or other markers of tissue oxygenation have been implemented [40-42], but nobody demonstrated it for dynamic exercise at 7T and radial acquisition was also never implemented for these studies. These studies were conducted to investigate reactive hyperemia mostly.

Herein, we implemented novel interleaved golden angle radial MRI acquisition to simultaneously quantify muscle perfusion and T_2* at 7T, and demonstrate assessment of spatial and temporal changes in these parameters within calf muscle during recovery from plantar flexion exercise. The high magnetic field offers improvement in signal to noise ratio and radial acquisition, which is used for projection reconstruction of MR images, has the advantage of low sensitivity to human movement inside the scanner.

Different studies have demonstrated that skeletal muscle perfusion dynamics are capable of providing insights in pathological and physiological functions as well [43-46]. In these studies perfusion measurement reflects integrated function of respiratory, vascular and cardiovascular systems. Perfusion has been studied for functional hyperemia [47, 48] and reactive hyperemia [49]. As T_2* change has the potential to reflect the change of biochemichal components in organs, so it has been studied for diagnosis of several diseases [50]. T_2* study has also been of particular

interest to quantify Iron deposition in tissues [51], identifying the differentiation of different tumors and detecting its paramagnetic substance [52, 53].

Studies on combined quantification of perfusion and T_2* or other markers of tissue oxygenation have been implemented for reactive hyperemia [54-56] , but nobody demonstrated it for dynamic exercise at 7T. Also, functional hyperemia is more physiologically analogous to the demand of daily living than reactive hyperemia. High magnetic field of 7T and the advantage of radial acquisition having low sensitivity to bulk motions can result in measurement of perfusion and T_2* simultaneously with higher accuracy in skeletal muscle.

Herein, we implemented novel interleaved golden angle radial MRI acquisition to simultaneously quantify muscle perfusion and T_2* at 7T, and demonstrate assessment of spatial and temporal changes in these parameters within calf muscle during recovery from plantar flexion exercise. We further demonstrated the assessment of spatial and temporal changes in perfusion and T_2* in calf muscle during recovery from plantar flexion exercise.

Chapter 6

Methods

6.1 Centering the Radial Projections by Shift Estimation and Correction

When different gradients are applied during radial data acquisition, there is a time delay between the requested and actual starting time of the gradient waveform [57]. Because of this gradient delay, the center of acquired radial projections are shifted from the actual center of the kspace.

In Cartesian acquisition these shifts do not create any artifact in the image because all phase encoding lines have the same readout direction. So only the phase of the reconstructed image has an added linear phase gradient. But in radial acquisition readout directions are different for every acquisition angle. When the gridding is done and the image is reconstructed by Fourier transform, there is an artifact in the image.

To correct the shift of the center of radial spokes [58], calibration data at 0^o and 180^o (Figure 6.1), 90^o and 270^o (Figure 6.2) are acquired. The 0^o and 180^o radial spokes are on the same line but in opposite direction. We flip one of the two spokes and plot the magnitude of both spokes. If there was no shift in the acquired radial lines, then they would be exactly on the top of each other. To estimate the shift along $k_y=0$ line, 0^o and 180^o spokes are used and for the shift along $k_x=0$ line, 90^o and 270^o spokes are used. As we know from the FT property, if there is a shift between the two signals in kspace, then there would be a linear phase ramp between those two signals in spatial domain. The steps to calculate the shift along $k_y=0$ line are described below:

1. Flip one of the 0^o and 180^o spokes.
2. Take the FT of the magnitude of two spokes.
3. Calculate and plot the phase difference between these two signals. It will show up as a linear region at the central potion. This is the portion we are interested in because the center portion of radial kspace line carries most signal information.
4. Fit the central linear portion to a linear equation and calculate the slope of that line.
5. Shift along $k_y=0$ line in terms of sample is calculated from the slope from the equation: Δk_x=-slope × no. of samples/4π.

Same procedure is used with 90^o and 270^o spokes to calculate Δk_y along $k_x=0$ line. Then shift along every radial spoke can be calculated using the equation [59] :

$$\Delta k(\Theta)= \Delta k_x \cos^2(\Theta)+ \Delta k_y \sin^2(\Theta) \text{ ; for every angle } \Theta.$$

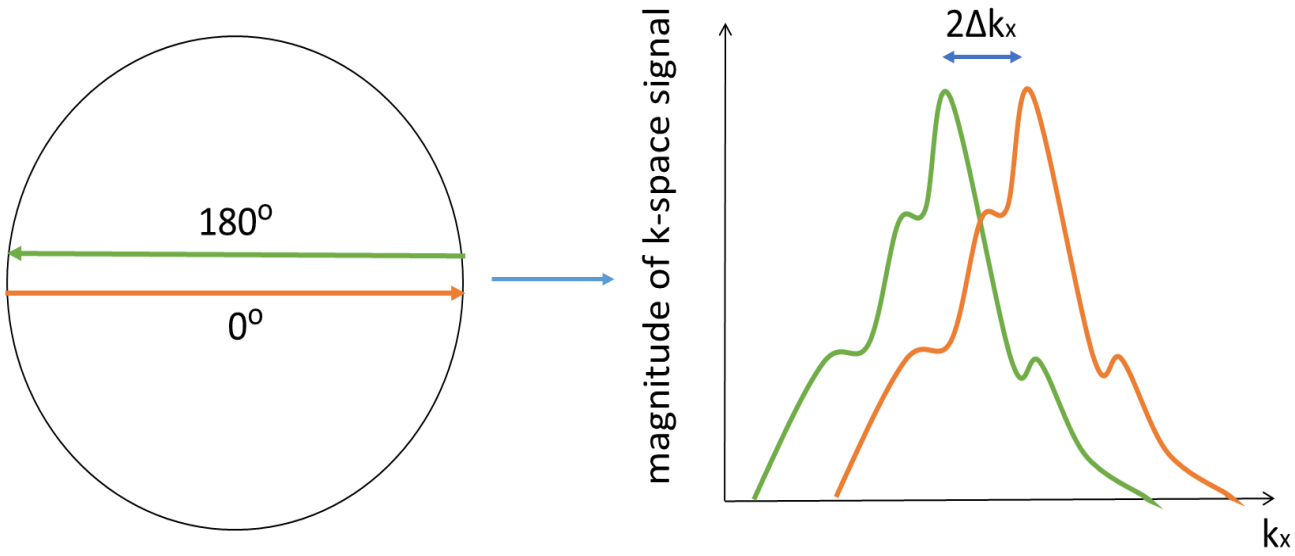

Figure 6.1: Gradient correction for k_x with 0^o and 180^o radial spokes.

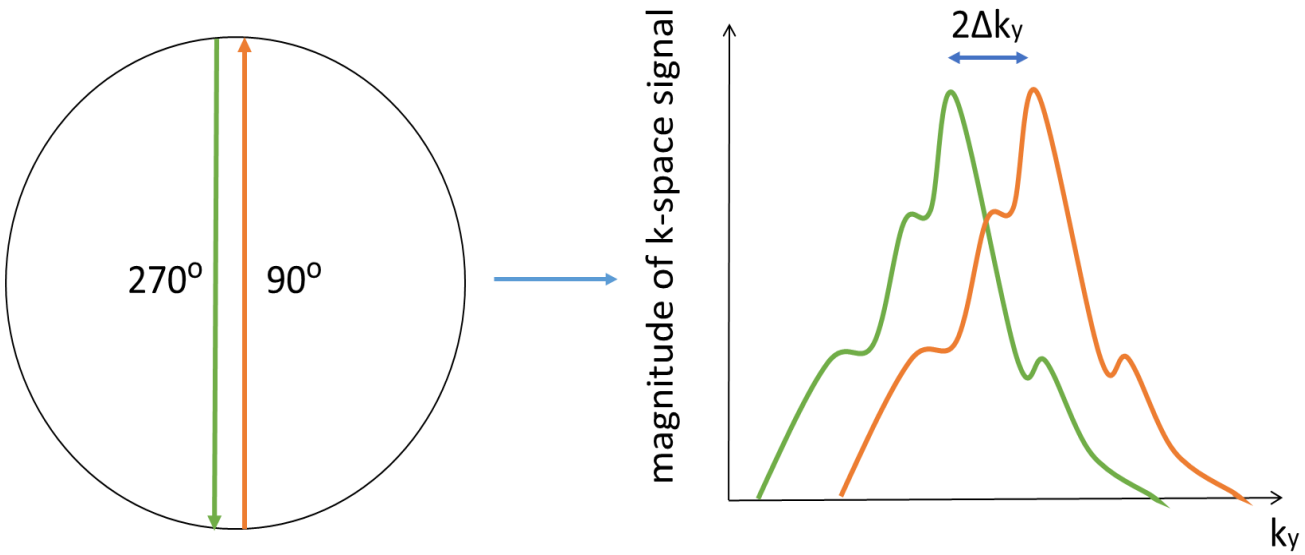

Figure 6.2: Gradient correction for k_y with 90^o and 270^o radial spokes.

6.2 In Vivo Study Design

The study was approved by Auburn University institutional review board. MR studies were performed on a Siemens 7T system (Erlangen, Germany) using a surface coil. Informed consent was provided by each subject prior to participation in the study. Seven subjects participated in the study. First one minute scan was done when the subjects were resting. The subjects then performed 2 minutes of plantar flexion at 0.5 Hz against a resistance of 40% of MVC. After that, data was acquired for almost 3 minutes in recovery.

6.3 Imaging Sequence

Pulse sequence was developed to acquire data simultaneously from two different slices. Arterial spin labeling sequence SATIR [60] was implemented using hyperbolic secant inversion pulse for spin tagging and golden angle radial readout (Figure 6.3a - slice 1). Time delay between perfusion tagging and acquisition was used for interleaved acquisition of T_2* data for a slice located 3 cm distally from the perfusion slice (Figure 6.3a – slice 2). A multi-echo radial GRE sequence with radial acquisition was used for T_2* mapping (Figure 6.3b). Temporal resolution for perfusion and T_2* was approximately 1.3 seconds.

Quantitative perfusion and T_2* maps were acquired at rest. Common acquisition parameters: FOV = 192 mm, slice thickness = 5 mm, TR = 1.28 s, Flip angle = 15º and 64 radial projections.

Resting perfusion measurements were acquired with a slice selective and nonselective tagging pulse with tagging time = 1 sec. T_2* was acquired with TEs = 2.2, 5.0, 7.8, 10.6 and 13.4 ms. Quantitative perfusion maps were determined as described before [61]. T_2* was calculated by fitting a mono-exponential function to magnitude signal intensity.

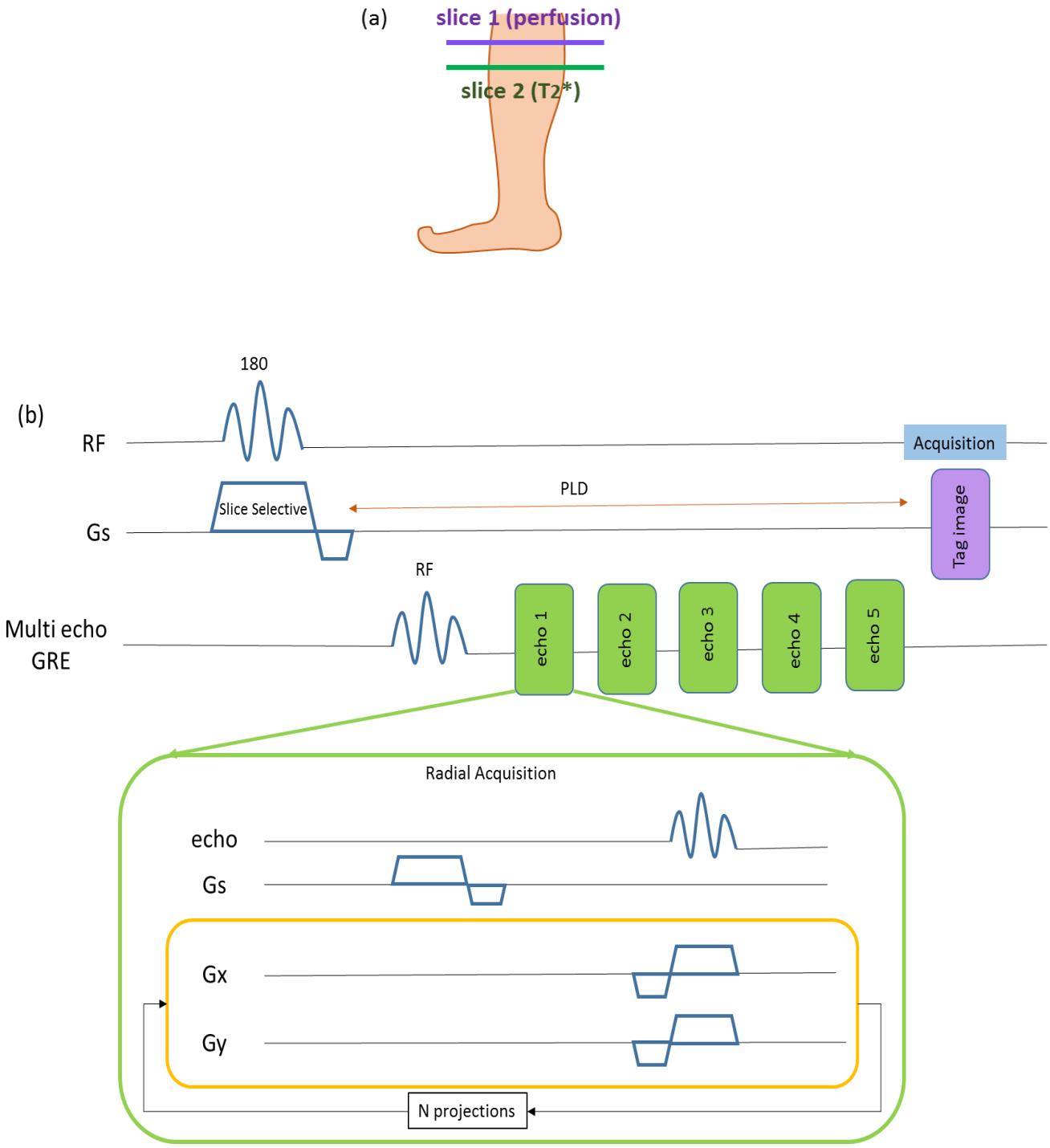

Figure 6.3: Perfusion and T_2* slice locations on calf muscle (a) and pulse sequence for data acquisition (b). Slice selective 180^o inversion RF pulse was applied for acquiring the tag image in slice 1. During the post labeling delay (PLD) after this pulse, multi echo GRE sequence with radial acquisition applied in slice 2 to acquire 5 echo images for T_2* quantification. After PLD tag image with radial acquisition was acquired at slice 1.

6.4 Phantom Experiment

Developed pulse sequence was validated by phantom experiments first. Agar, Agarose and Copper Sulfate solutions were prepared for the phantom experiment. 0.5, 1, 2, 3, 4 and 5 percent Agar and Agarose solutions were prepared in 50 mL test tubes. Also, 0.5, 1, 2, 3, 4 and 5 mM Copper Sulfate solutions were prepared in 50 mL test tubes for the phantom experiments.

T_2* and perfusion were measured by the developed pulse sequence using the same protocol as mentioned before. T_2* was also measured by standard multi echo GRE sequence only and perfusion was measured by SATIR sequence only. Images acquired in coronal plane were used for the phantom study.

T_2* from multi echo GRE sequence only and developed sequence were compared to test the validity of the sequence. Also, both cartesian and golden angle radial acquisition were implemented in the developed pulse sequence to examine if there is any difference in the result.

6.5 Data Analysis

6.5.1 Perfusion

Perfusion weighted image at resting state was generated from the difference of two images acquired with slice selective and non-selective inversion pulses to identify the region where blood is highly perfused. The muscle area activated with high perfusion due to exercise was identified from the difference of the first and the last slice selective image acquired during the recovery period. From this muscle activation map a region of interest (ROI) was selected to calculate the

perfusion using the SATIR equation. Dynamic change in perfusion was measured as a change from the resting value during the recovery period.

6.5.2 T_2*

T_2* was calculated by fitting the signal intensities from five echo images to a mono-exponential equation. A T_2* map was generated for the resting state by evaluating the value of T_2* at every pixel location. The muscle area with decreased T_2* due to exercise was identified from the difference of the first and the last T_2* map generated during the recovery period. From this muscle activation map a region of interest (ROI) was selected to observe the relative change of T_2* which was normalized by the resting T_2* value.

Chapter 7

Results

7.1 Gradient Calibration and Correction

Prior to the actual phantom and human study, the reconstructed phantom images acquired with radial acquisition showed artifacts (Figure 7.4a). So gradient calibration and correction was needed. Calibration experiment was done with phantoms for off center imaging at 500 Hz bandwidth to be consistent with the actual study. As mentioned before, 0^o and 180^o calibration spoke resulted in a sample shift of 0.588 in k_x direction (Figure 7.1-7.3). Similarly 90^o and 270^o spokes resulted in a sample shift of 0.62 in k_y direction. Another set calibration data was acquired during the actual human study which resulted in $\Delta k_x = 0.578$ and $\Delta k_y = 0.617$, which is pretty close to the phantom results. From the shifts along k_x and k_y , sample shift along radial spokes at every angle was calculated and corrected. Corrected phantom image is shown in Figure 7.4b.

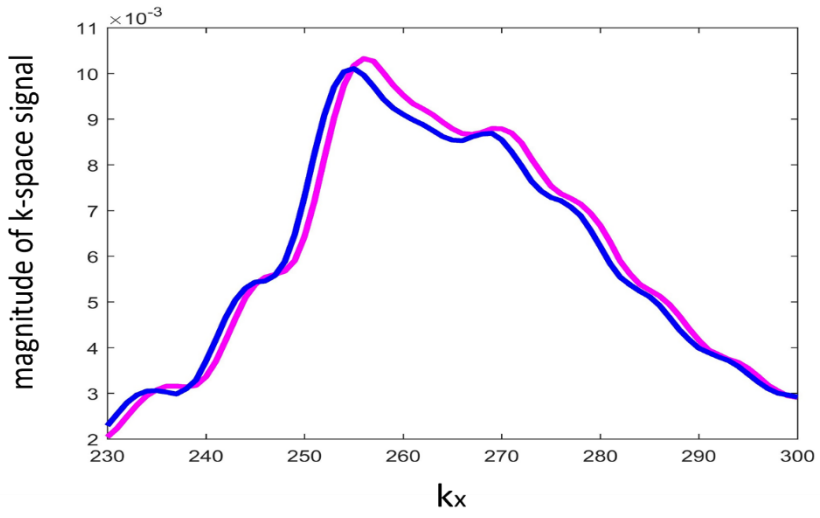

Figure 7.1: Magnitude plot of 0^o and flipped 180^o radial spokes.

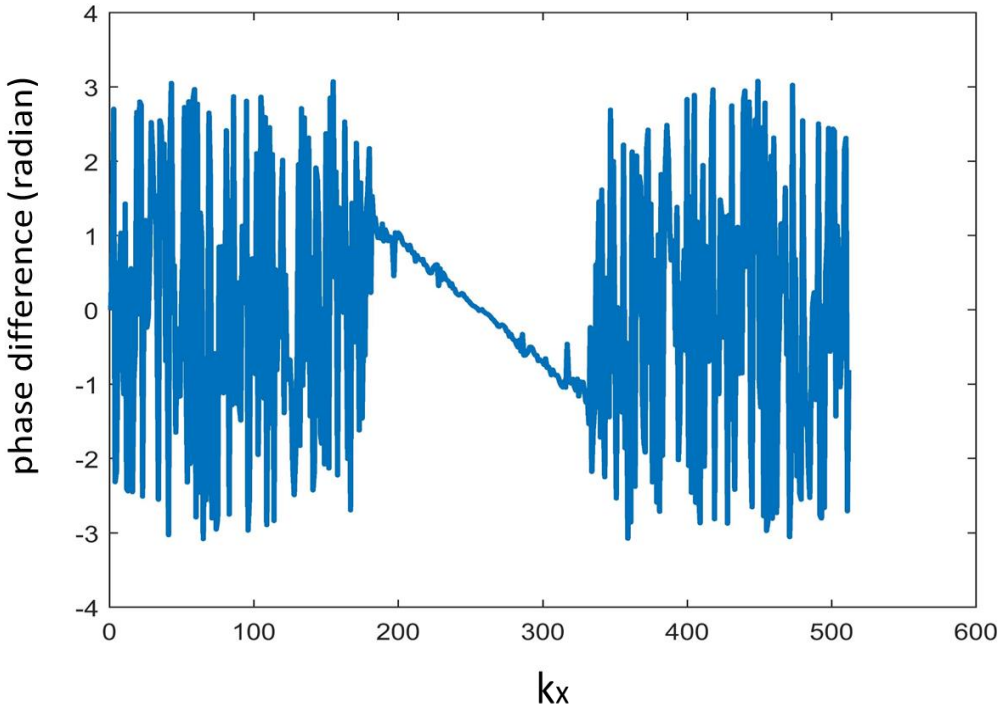

Figure 7.2: Phase difference between 0^o and flipped 180^o radial spoke magnitudes.

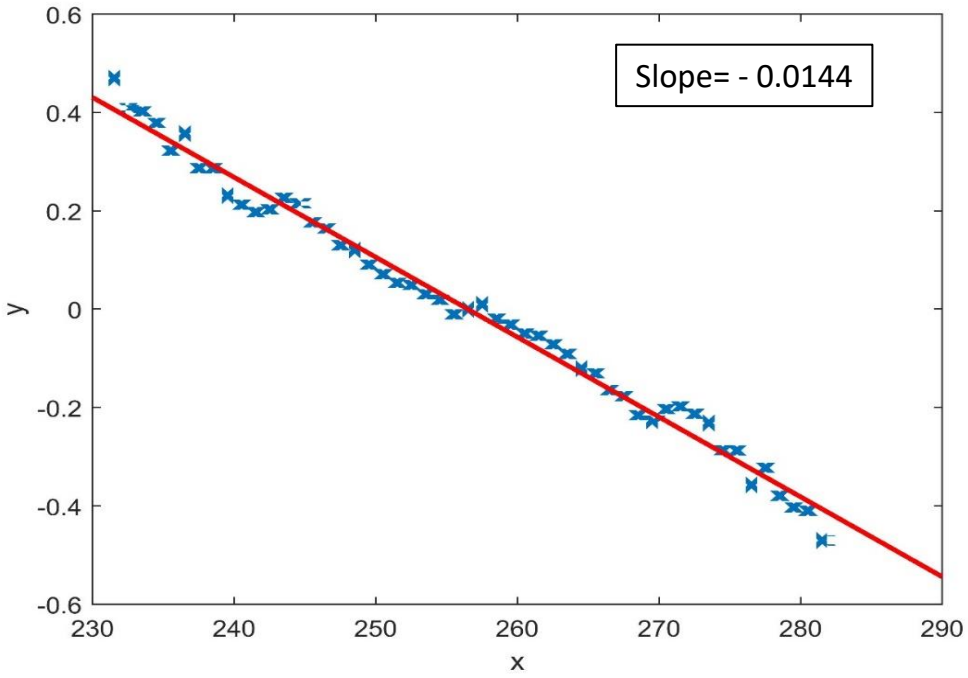

Figure 7.3: Fitting of the linear phase ramp portion to a linear equation to calculate Δk_x.

(a)

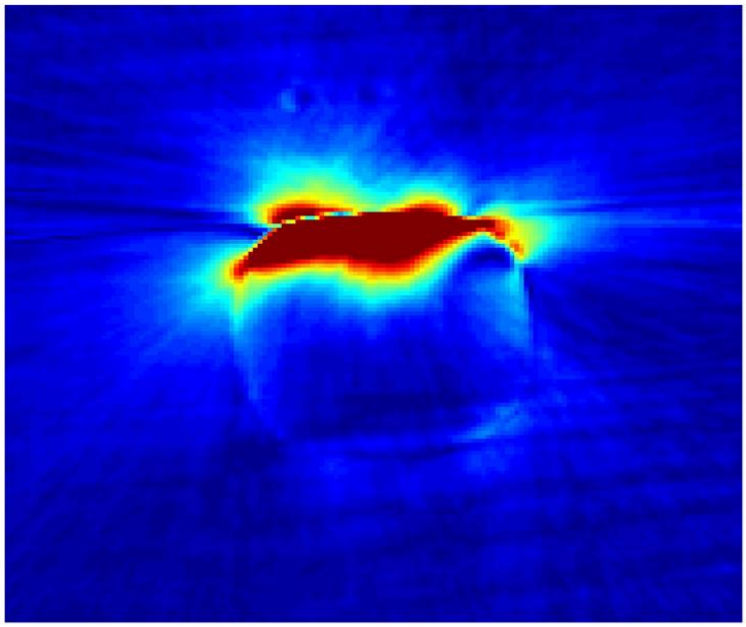

(b)

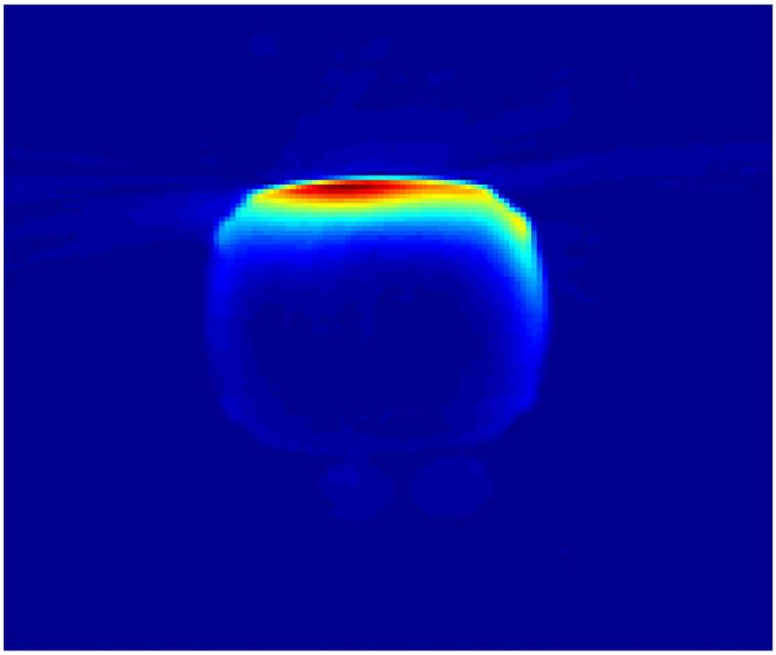

Figure 7.4: Phantom image reconstructed without shift correction (a) and with shift correction (b).

7.2 Phantom Study

The five echo images of agar phantom are shown In the Figure 7.5, where green ROI represents 1% agar solution, the intensity of which from five echo images were fitted to a mono exponential equation to calculate the T_2* by all three methods. T_2* of selected ROI was 45.6 ms from multi echo GRE sequence, 43.9 ms from cartesian acquisition using developed sequence and 44.2 ms from radial acquisition using developed sequence.

As there was almost no perfusion in the phantom experiments, so the quantitative perfusion was approximately zero for the phantom experiments from both SATIR sequence and developed sequence.

Figure 7.6a shows that T_2* values acquired by both standard sequence and developed sequence are pretty close. Figure 7.6b shows these values have a very good coefficient of determination of 0.98.

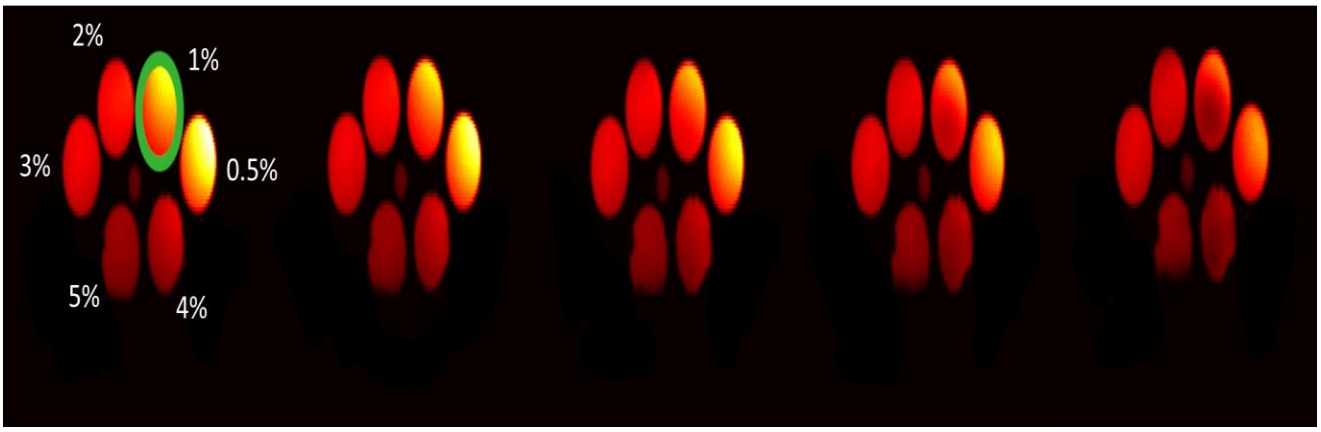

Figure 7.5: In this figure 5 echo images from the phantom experiment are shown that are used for the intensity fitting to a mono-exponential equation to calculate T_2*. Perfusion weighted image shows up blank as there is almost no perfusion in the phantom experiment.

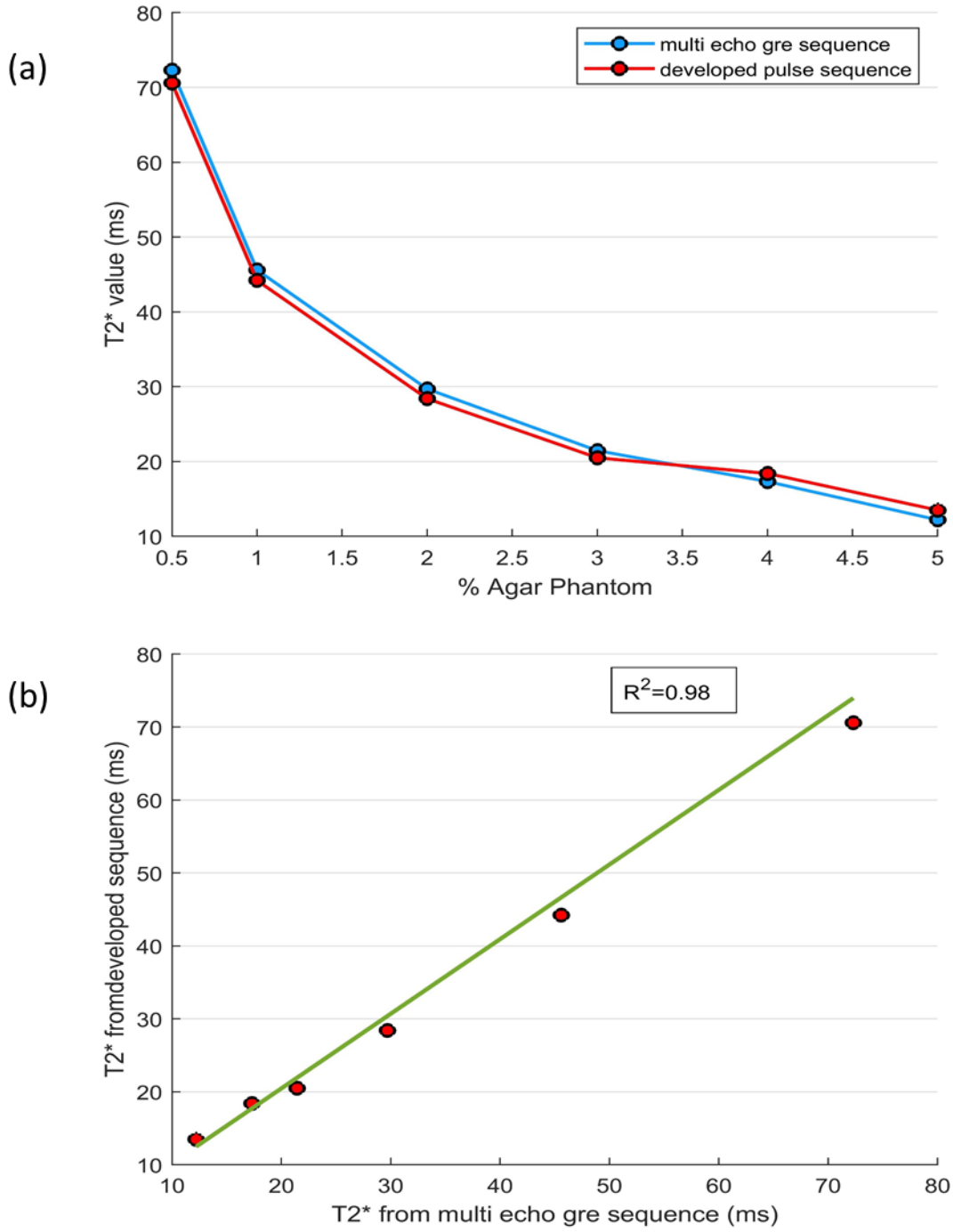

Figure 7.6: T_2* values of Agar phantoms of different concentrations using both multi echo GRE sequence and our developed sequence (a) and validation of the results with coefficient of determination (b).

7.3 Perfusion

Anatomical image at slice location 1 (Figure 7.7) and corresponding representative slice selective perfusion weighted image at rest are shown in Figure 7.8. Blood vessels on perfusion images show high signal due to flow. From the resting perfusion weighted image we see that the gastrocnemius muscle has the highest perfusion in the calf at rest. At rest the perfusion was 5 ± 2 mL/min/100g. Figure 7.10 shows change in perfusion for one subject immediately after exercise indicating regions of muscle activation. This overlay map is change from the resting state. The overlay map indicate that immediately after the exercise perfusion is increased in the gastrocnemius muscle. A region of interest (ROI) corresponding to the activated muscle regions identified on the perfusion maps was manually traced on the images.

ROI analysis showed that perfusion was significantly increased reaching 80 ± 10 mL/min/100g immediately after exercise. Figure 7.12 shows average perfusion with standard deviation during recovery period from exercise for all subjects. Perfusion recovered slowly during post-exercise rest period and average time to return to baseline was approximately 120 s. As exercise is performed, oxygen is extracted from the blood causing hemoglobin deoxygenation. So oxygenated blood flows into that region and perfusion increases.

Figure 7.14 shows the synopsis of change in perfusion in different muscle groups- gastrocnemius, soleus and peronius muscles within calf muscle during recovery from exercise.

7.4 T_2*

Anatomical image at slice location 2 (Figure 7.7) and corresponding representative slice selective T_2* map at rest are shown in Figure 7.9. From resting T_2* map we see that tibialis posterior muscle and gastrocnemius muscle exhibit high T_2*. Average baseline T_2* was 21 ms in gastrocnemius muscle at rest. Figure 7.11 shows change in T_2* for one subject immediately after exercise indicating regions of muscle activation. The overlay map indicate that immediately after the exercise T_2* is decreased in the gastrocnemius muscle. A region of interest (ROI) corresponding to the activated muscle regions identified on the T_2* maps was manually traced on the images. Shim difference between experiments affects baseline (resting) T_2*; therefore post exercise T_2* was normalized to the resting map from each individual. T_2* in the selected ROI decreased by approximately 8 ± 3 % immediately after exercise from the resting value. T_2* recovery showed exponential behavior. Figure 7.13 shows average normalized T_2* with standard deviation during recovery period from exercise for all subjects.

T_2* decrease immediately after plantar flexion is mainly induced by hemoglobin deoxygenation. At low values of blood oxygen saturation, an increase of blood volume results in a decrease of T_2*. As oxygen supply is increased with increased oxygenated blood flow, T_2* slowly increases and returns to its resting value.

Figure 7.15 shows the synopsis of change in T_2* in different muscle groups- gastrocnemius, soleus and peronius muscles within calf muscle during recovery from exercise. The peroneus muscle is not much effected by the exercise as it shows kind of random changes in T_2*. But gastrocnemius and soleus muscles exhibit significant change in T_2* due to exercise.

Table 7.1: Perfusion and T_2* values of all the subjects.

Subject	***Perfusion***		***T_2****	
	Peak flow (mL/min/100g)	Recovery time (sec)	Baseline T_2* (ms)	Minimum relative T_2*
1	83	112	20.49	0.93
2	86	131	21.23	0.951
3	70	103	23.27	0.923
4	77	125	24.58	0.917
5	74	118	19.73	0.91
6	89	140	22.25	0.89
7	71	123	18.31	0.94

Figure 7.7: Two slice locations for perfusion and T_2* on calf muscle. Slice 1 is perfusion slice and slice 2 is T_2* slice.

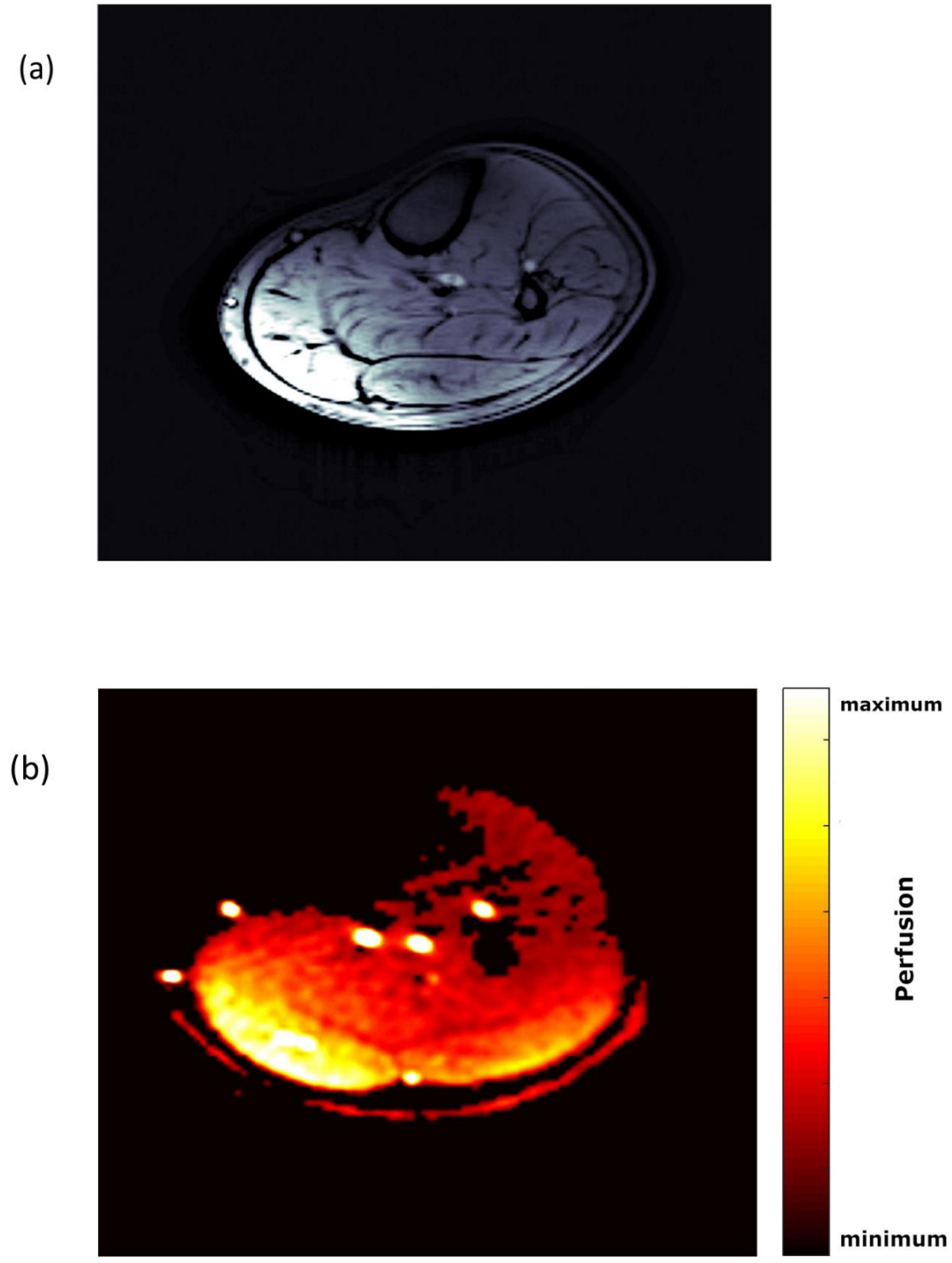

Figure 7.8: Anatomical image of perfusion slice (a) and perfusion weighted image of the same slice (b) at rest.

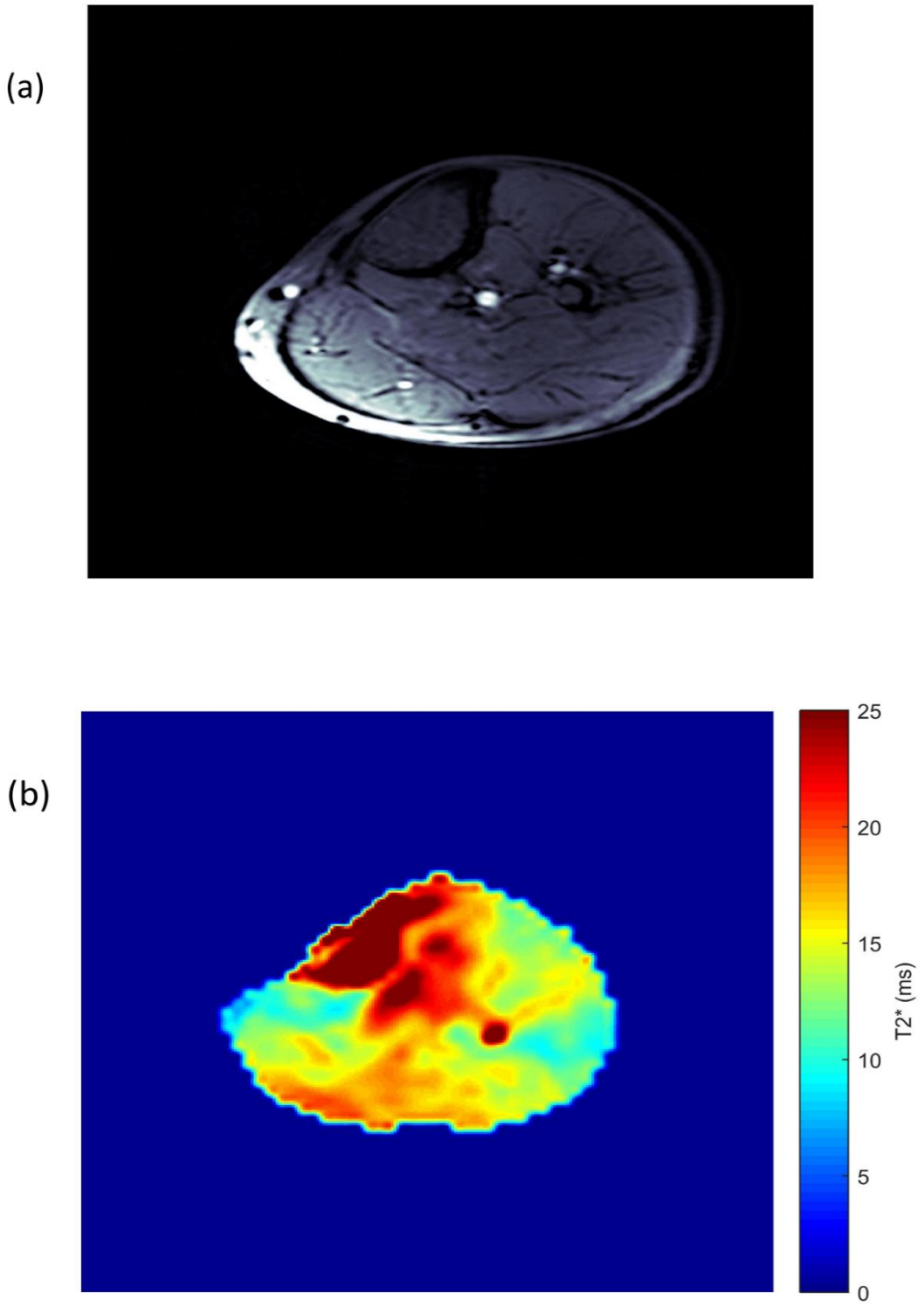

Figure 7.9: Anatomical image of T_2* slice (a) and T_2* map of the same slice (b) at rest.

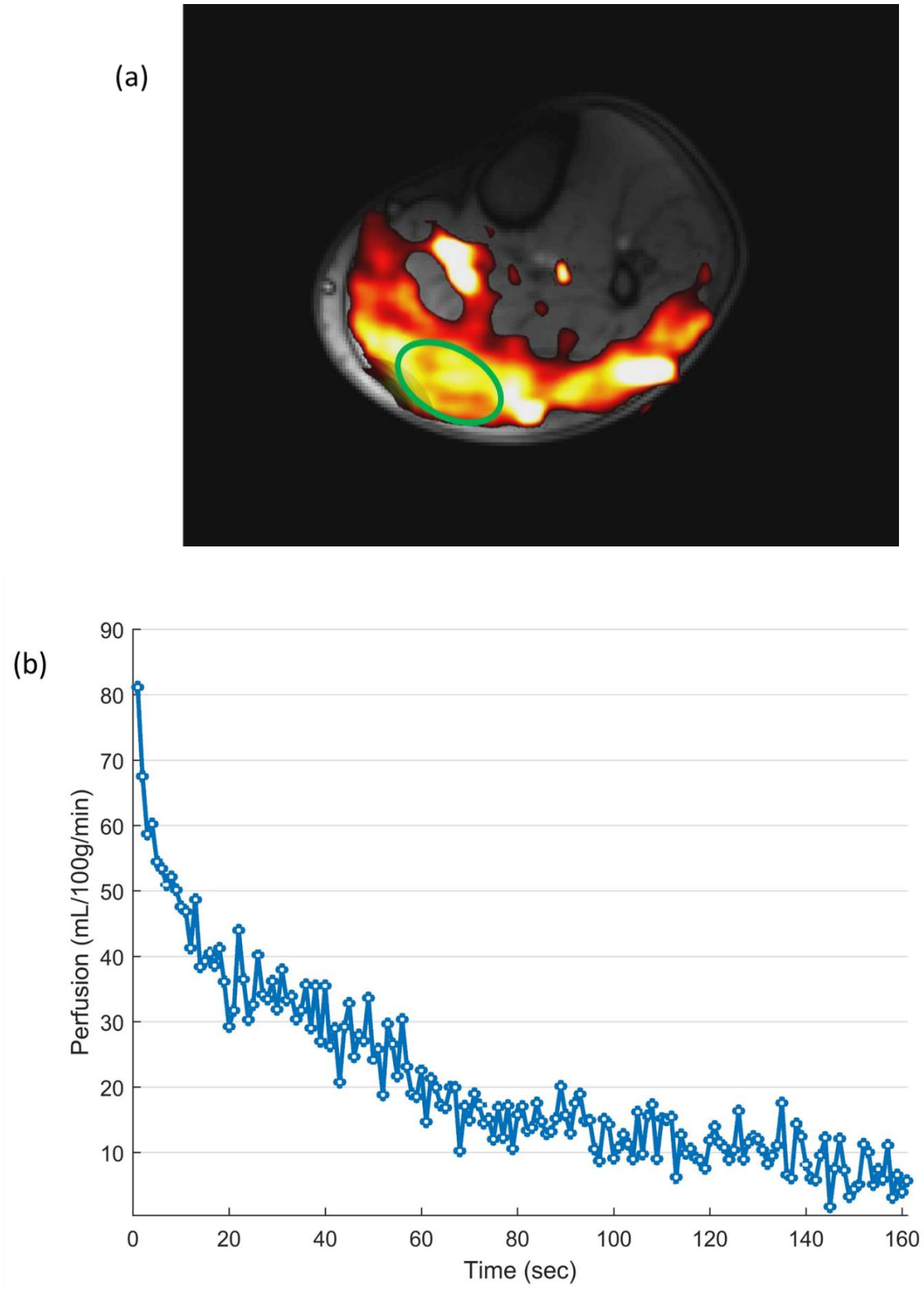

Figure 7.10: Increased perfusion activated area (a) and plot of perfusion (b) from selected ROI in activated region of slice of one subject during recovery from exercise.

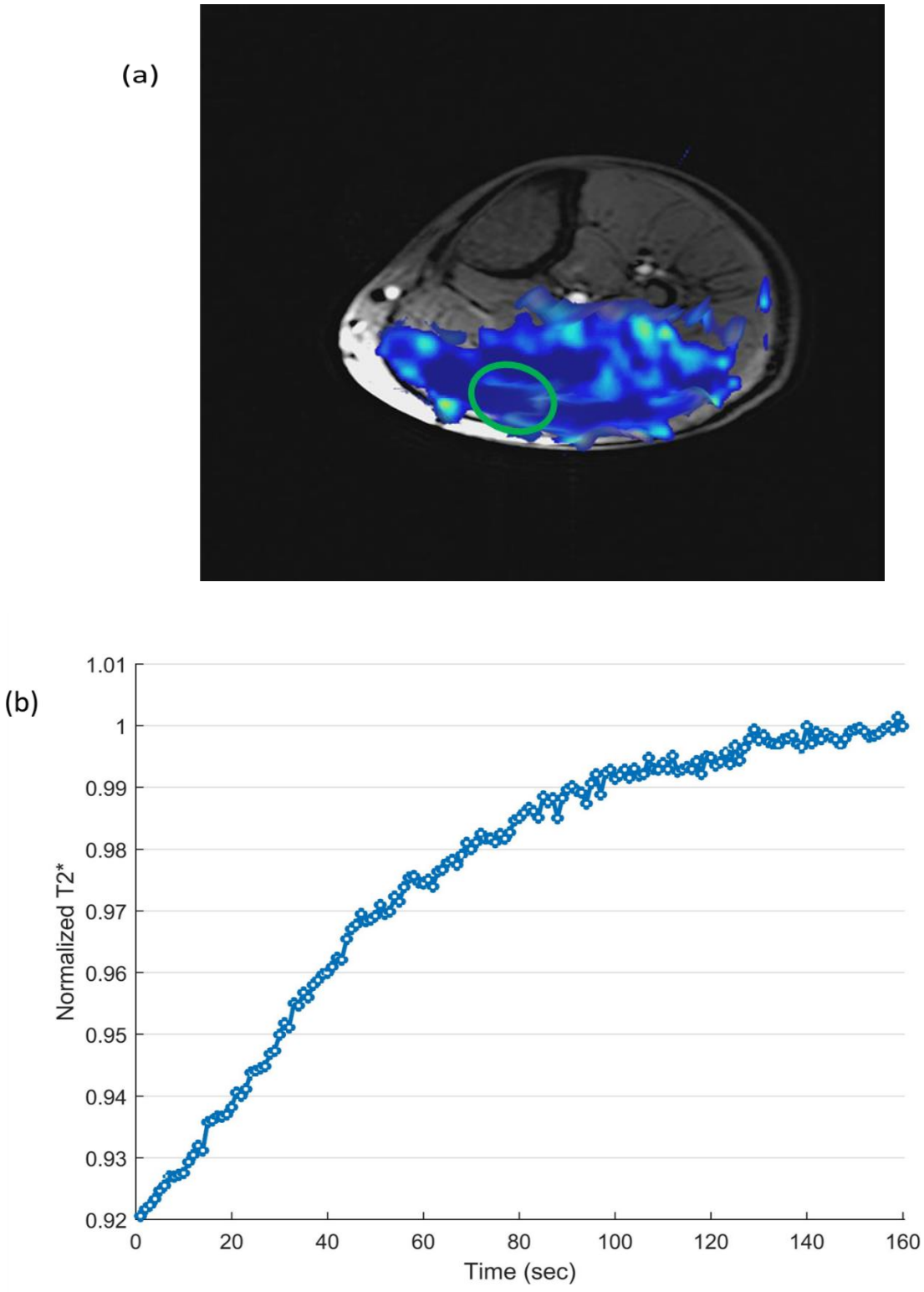

Figure 7.11: Decreased T_2* activated area (a) plot of relative T_2* (b) from selected ROI in activated region of slice of one subject during recovery from exercise.

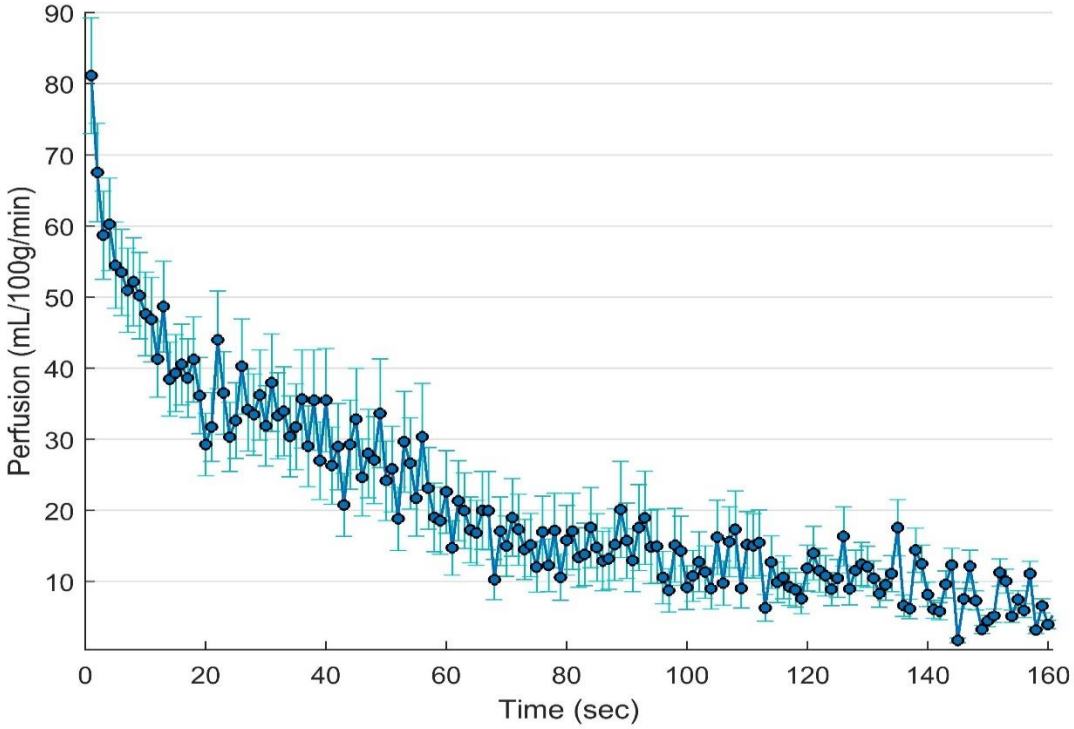

Figure 7.12: Average perfusion with standard deviation of all the subjects during recovery perod.

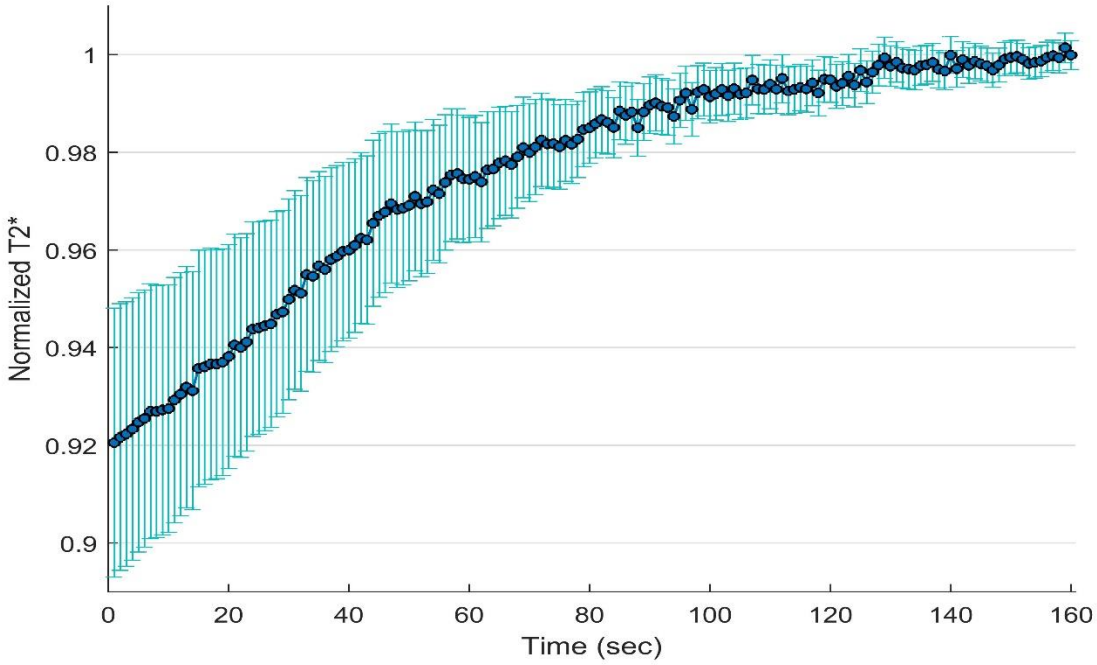

Figure 7.13: Average relative T_2* with standard deviation of all subjects during recovery period.

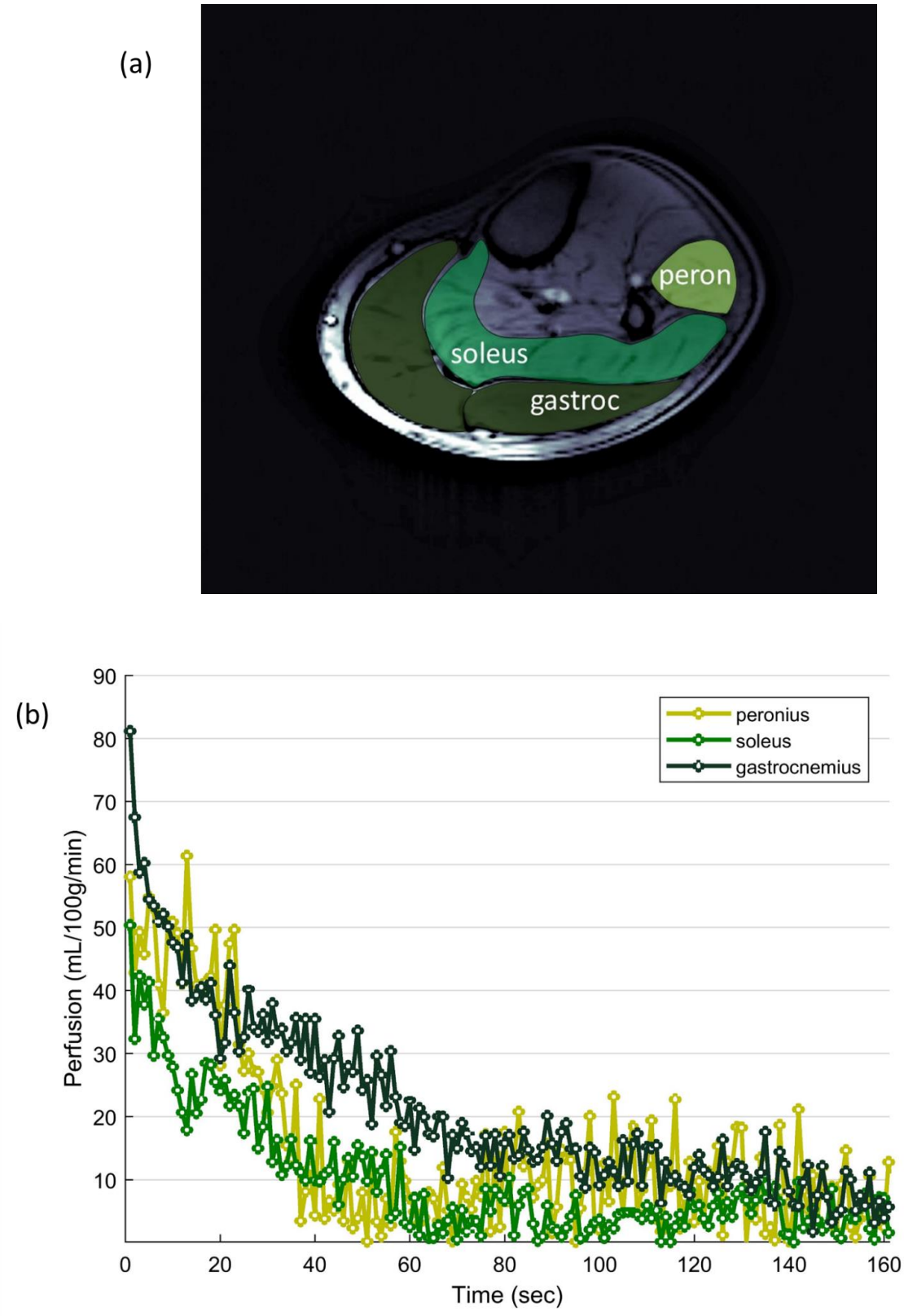

Figure 7.14: Different muscle groups in perfusion slice (a) and corresponding muscle perfusion (b) during recovery period.

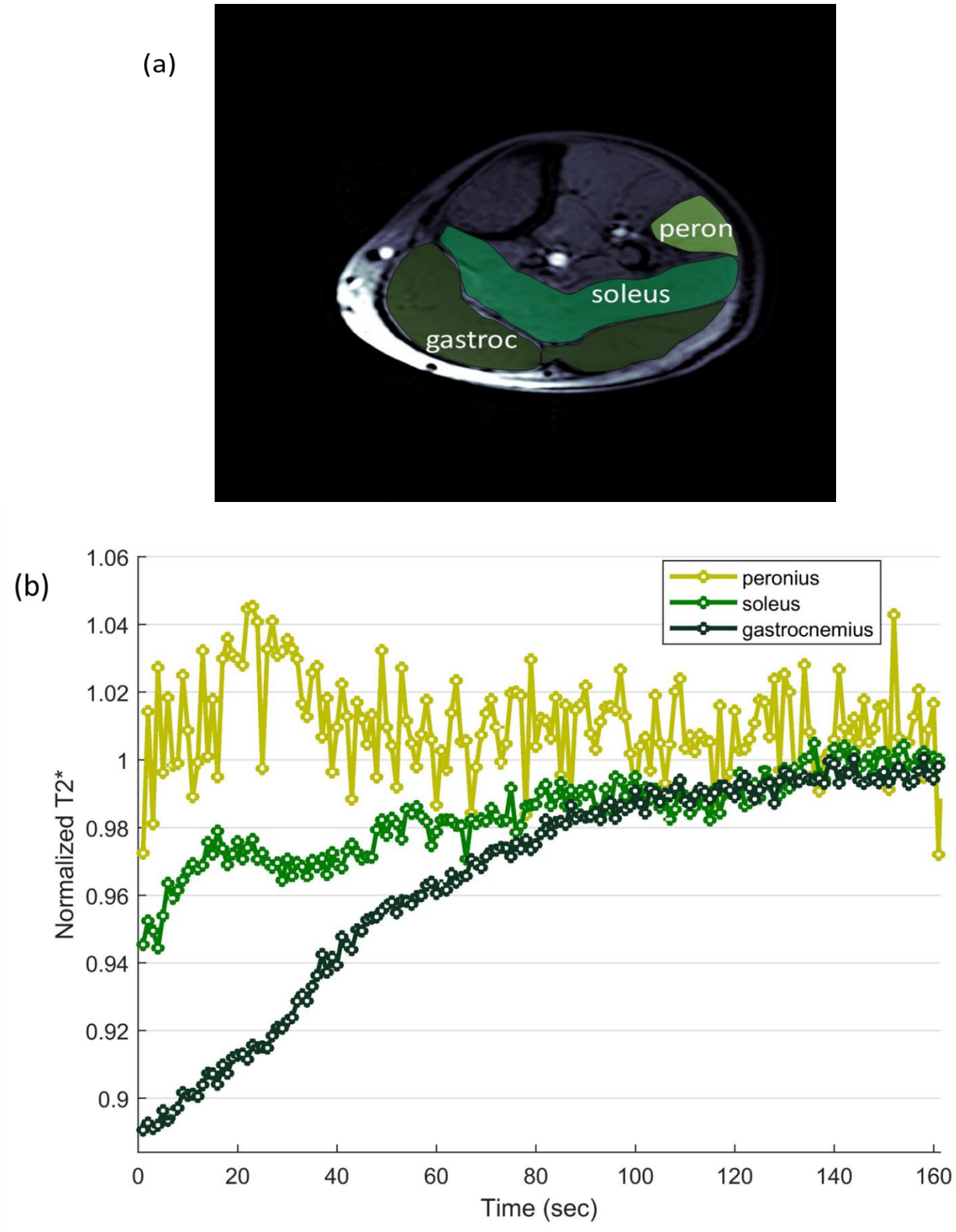

Figure 7.15: Different muscle groups in T_2* slice (a) and corresponding muscle T_2* (b) during recovery period.

Chapter 8

Discussion

8.1 Repeatability

Twelve studies were performed with the developed pulse sequence. As mentioned before, six of them were young healthy subjects and six of them were old healthy subjects. The results are in good agreement with a small range of variability. The variability was probably caused by the amount of exercise that was being performed. Some of the subjects might not be capable of doing the required amount of exercise. Oxygen consumption rate plays an important role as well.

8.2 Perfusion

As exercise is performed, oxygen is extracted from the blood. So new oxygenated blood flows into that region and perfusion increases. In vPIVOT study, peak perfusion was reported as almost 73 mL/min/100g after plantar flexion exercise against a pressure of 10 psi every second, leading to a power of 6W at 3T in gastroc muscle [62] which is pretty close to our result.

Another related study was done to quantify perfusion with dynamic exercise [63], where one subject did plantar flexion exercise at 20 %, 40 % and 60 % of MVC at 7T. They reported peak perfusion of almost 37 mL/min/100g and 68 mL/min/100g for 40 % and 60 % MVC respectively, which is lower than our result. The first reason behind this is they used T1=2.587 s [64] at 7T and also used simplified general kinetic model [65] to calculate perfusion. In our study, we used

T1=2.087 s [66] at 7T which was reported in a more recent study using more optimal sequence. Just by using this value for T1 in that simplified general kinetic model, the value of perfusion is increased by almost 15 % for the PLD (or inflow time) of 1.5 sec used in their study. The second reason for this is they measured the average peak perfusion of whole gastrocnemius muscle and we measured the peak perfusion of a selected ROI where perfusion is high within the gastrocnemius muscle instead of the whole muscle. Another possible factor might be that study used EPI sequence whereas our study used radial acquisition.

The perfusion immediately after the exercise measured in this study was higher than what was reported in SATIR protocol for plantar flexion [67]. It was 50 ± 12 mL/min/100g in that study which is almost 20 mL/min/100g smaller than our result. The reason might be that study was conducted with a very short plantar flexion exercise and the exercise was in anaerobic condition. Another important fact is whole leg perfusion was quantified in this study and the study was done at 3T. So the perfusion peak was different.

Perfusion reported for reactive hyperemia by PIVOT [68] and SATIR had a peak perfusion of 37 ± 6.1 mL/min/100g and 50 ± 13 mL/min/100g respectively, which are also lower than our peak perfusion value due to plantar flexion at 40% MVC. Obviously this is because of reactive hyperemia, which is a different study than dynamic exercise. And also, these studies were on the whole leg perfusion and on soleus muscle, not on gastrocnemius muscle. These studies were done at 3T. Temporal resolution of these studies was 2 seconds, where temporal resolution of our study is 1.3 seconds.

8.3 T_2*

The baseline T_2* value matched fairly with the previous study in calf muscle at 7T [69]. T_2* decrease immediately after plantar flexion is mainly induced by hemoglobin deoxygenation. As exercise is performed, oxygen is extracted from the muscle and results in hemoglobin deoxygenation. This changes the magnetic susceptibility and paramagnetism of deoxyhemoglobin causes local magnetic field inhomogeneity. As the oxygen saturation decreases, concentration of deoxyhemoglobin increases. This causes the T_2* to decrease. At low values of blood oxygen saturation, an increase of blood volume results in a decrease of T_2*. As new oxygenated blood flows into this muscle region, the oxyhemoglobin causes the T_2* to increase again.

In vPIVOT study lowest relative T_2* was reported as almost 0.97 after plantar flexion exercise against a pressure of 10 psi every second, leading to a power of 6W at 3T in gastroc muscle [70] which is pretty close to our result. The response of T_2* recovery is also similar to our findings. The result also fairly matches with the PIVOT study except the huge peak in relative T_2* after the minimum value. That is because that study was done for reactive hyperemia and the leg was cuffed. So there was almost no blood flow. When the cuff was released, there was a huge inrush blood flow that caused the T_2* to reach a maximum peak higher than 15% of its resting value. But in dynamic exercise at 40 % MVC blood flow is not zero. So the T_2* do not exhibit any peak and slowly recovers to its resting value exponentially.

Chapter 9

Conclusion

This study demonstrates the ability to simultaneously quantify skeletal muscle perfusion and T_2*, both at rest and dynamically, for post exercise recovery in calf muscle at 7T. An interleaved golden angle radial acquisition pulse sequence was implemented for the study which helps reduce bulk motion artifacts. The temporal and spatial resolution of the protocol was sufficient to measure changes in metabolism-related parameters post exercise. Dynamic plantar flexion exercise isolates the calf muscles and might provide valuable insight into pathophysiological processes independent of impaired heart function. Accordingly, the information provided by this technique may prove to be very valuable in understanding muscle metabolism in healthy subjects as well as patient populations who experience mobility disability.

References

[1] Steven Sourbron, Technical aspects of MR perfusion, European Journal of Radiology, 2010; 76:304–313.

[2] Geon-Ho Jahng, Ka-Loh Li, Leif Ostergaard, Fernando Calamante, Perfusion Magnetic Resonance Imaging: A Comprehensive Update on Principles and Techniques, Korean J Radiol 2014;15(5):554-577.

[3] Christopher P. Elder, Ryan N. Cook, Marti A. Chance, Elizabeth A. Copenhaver, and Bruce M. Damon, Image-Based Calculation of Perfusion and Oxyhemoglobin Saturation in Skeletal Muscle During Submaximal Isometric Contractions. Magnetic Resonance in Medicine, 2010; 64:852–861.

[4] Wu W-C, Mohler E, Ratcliffe SJ, Wehrli FW, Detre JA, Floyd TF. Skeletal muscle microvascular flow in progressive peripheral artery disease: Assessment with continuous arterial spin-labeling perfusion magnetic resonance imaging. JACC 2009;53:2372–2377.

[5] Gr€ozinger G, Pohmann R, Schick F, et al. Perfusion measurements of the calf in patients with peripheral arterial occlusive disease before and after percutaneous transluminal angioplasty using MR arterial spin labeling. J Magn Reson Imaging 2013;40:980–987.

[6] Englund EK, Langham MC, Ratcliffe SJ, et al. Multiparametric assessment of vascular function in peripheral artery disease: dynamic measurement of skeletal muscle perfusion, blood-oxygen level dependent signal, and venous oxygen saturation. Circ Cardiovasc Imaging 2015; 8:e002673 e002673.

[7] Anderson JD, Epstein FH, Meyer CH, et al. Multifactorial determinants of functional capacity in peripheral arterial disease: uncoupling of calf muscle perfusion and metabolism. JACC 2009;54:628–635.

[8] Sorensen AG, Buonanno FS, Gonzalez RG, et al. Hyperacute stroke: evaluation with combined multisection diffusion weighted echo planar MR imaging. Radiology 1996;199:391 -401.

[9] M. Barzin, M. Kowsarian, S. Akhlaghpoor, R. Jalalian, and M. Taremi, Correlation of cardiac MRI T2* with echocardiography in thalassemia major, European Review for Medical and Pharmacological Sciences, 2012; 16(2): 254–260.

[10] T. Kim, T. Murakami, M. Hori, H. Onishi, K. Tomoda, and H. Nakamura, Effect of superparamagnetic iron oxide on tumor-to-liver contrast at T2*-weighted gradient-echo MRI: comparison between 3.0 T and 1.5 T MR systems, Journal of Magnetic Resonance Imaging, 2009;. 29(3): 595–600.

[11] A. N. Tong, X. Y. Lv, P. Yan, and Y. M. Wang, Magnetic resonance T2*-weighted study of U87 MG glioma tumors and its relationship between tumor hypoxia and VEGF expression, CNS Neuroscience and Therapeutics, 2013; 19(3): 201–203.

[12] Vogt FM, Herborn CU, Goyen M. MR venography. Magn Reson Imaging Clin N Am. 2005;13(1):113-29.

[13] Rosen BR, Belliveau JW, Vevea JM, Brady TJ. Perfusion imaging with NMR contrast agents. Magn Reson Med 1990;14:249-265.

[14] Erlemann R, Reiser MF, Peters PE, Vasallo P, Nommensen B, Kusnierz-Glaz CR, et al. Musculoskeletal neoplasms: static and dynamic Gd-DTPA--enhanced MR imaging. Radiology 1989;171:767-773.

[15] Detre JA, Leigh JS, Williams DS, Koretsky AP. Perfusion imaging. Magn Reson Med 1992;23:37-45.

[16] Wong EC. An introduction to ASL labeling techniques. J Magn Reson Imaging 2014;40:1 -10.

[17] Williams DS, Detre JA, Leigh JS, Koretsky AP. Magnetic resonance imaging of perfusion using spin inversion of arterial water. Proc Natl Acad Sci U S A 1992;89:212-216.

[18] Gr€ozinger G, Pohmann R, Schick F, et al. Perfusion measurements of the calf in patients with peripheral arterial occlusive disease before and after percutaneous transluminal angioplasty using MR arterial spin labeling. J Magn Reson Imaging 2013;40:980–987.

[19] Wu W-C, Wang DJ, Detre JA, et al. Hyperemic flow heterogeneity within the calf, foot, and forearm measured with continuous arterial spin labeling MRI. AJP Heart Circ Physiol 2008;294:H2129–H2136.

[20] Kim S-G. Quantification of relative cerebral blood-flow change by flow-sensitive alternating inversion-recovery (FAIR) technique: Application to functional mapping. Magn Reson Med 1995;34:293–301.

[21] Raynaud JS, Duteil S, Vaughan JT, et al. Determination of skeletal muscle perfusion using arterial spin labeling NMRI: validation by comparison with venous occlusion plethysmography. Magn Reson Med 2001;46:305–311.

[22] Edelman RR, Siewert B, Darby DG, Thangaraj V, Nobre AC, Mesulam MM, et al. Qualitative mapping of cerebral blood flow and functional localization with echo-planar MR imaging and signal targeting with alternating radio frequency. Radiology 1994;192:513-520.

[23] Kwong KK, Chesler DA, Weisskoff RM, Donahue KM, Davis TL, Ostergaard L, et al. MR perfusion studies with T1-weighted echo planar imaging. Magn Reson Med 1995;34:878-887.

[24] Kim SG. Quantification of relative cerebral blood flow change by flow-sensitive alternating inversion recovery (FAIR) technique: application to functional mapping. Magn Reson Med 1995;34:293-301.

[25] Wong EC, Buxton RB, Frank LR. Implementation of quantitative perfusion imaging techniques for functional brain mapping using pulsed arterial spin labeling. NMR Biomed 1997;10:237-249.

[26] Pruessmann KP, Golay X, Stuber M, Scheidegger MB, Boesiger P. RF pulse concatenation for spatially selective inversion. J Magn Reson 2000;146:58-65.

[27] Jahng GH, Zhu XP, Matson GB, Weiner MW, Schuff N. Improved perfusion-weighted MRI by a novel double inversion with proximal labeling of both tagged and control acquisitions. Magn Reson Med 2003;49:307-314.

[28] Jahng GH, Weiner MW, Schuff N. Improved arterial spin labeling method: applications for measurements of cerebral blood flow in human brain at high magnetic field MRI. Med Phys 2007;34:4519-4525.

[29] Wong EC, Cronin M, Wu WC, Inglis B, Frank LR, Liu TT. Velocity-selective arterial spin labeling. Magn Reson Med 2006;55:1334-1341.

[30] Elster AD. Gradient echo imaging: techniques and acronyms. Radiology 1993; 186:1-8.

[31] Kim SG. Quantification of relative cerebral blood flow change by flow-sensitive alternating inversion recovery (FAIR) technique: application to functional mapping. Magn Reson Med. 1995; 34:293–301.

[32] Kim SG, Tsekos NV. Perfusion imaging by a flow-sensitive alternating inversion recovery (FAIR) technique: application to functional brain imaging. Magn Reson Med. 1997; 37:425–35.

[33] Ogawa S, Menon RS, Tank DW, Kim SG, Merkle H, Ellermann JM, Uğurbil K. Functional brain mapping by blood oxygenation level-dependent contrast magnetic resonance imaging. A comparison of signal characteristics with a biophysical model. Biophys J. 1993; 64:803–12.

[34] Raynaud JS, Duteil S, Vaughan JT, Hennel F, Wary C, Leroy-Willig A, Carlier PG. Determination of skeletal muscle perfusion using arterial spin labeling NMRI: validation by comparison with venous occlusion plethysmography. Magn Reson Med. 2001; 46:305–11.

[35] Detre JA, Leigh JS, Williams DS, Koretsky AP. Perfusion imaging. Magn Reson Med 1992;23:37–45.

[36] Kim SG. Quantification of relative cerebral blood flow change by flowsensitive alternating inversion recovery (FAIR) technique: application to functional mapping. Magn Reson Med 1995;34:293–301.

[37] Jackson JI et al. Selection of a convolution function for fourier inversion using gridding. IEEE Trans Med Imaging 1991; 10(3): 473-478.

[38] Glover GH, Pauly JM. Projection reconstruction techniques for reduction of motion effects in MRI. Magn Reson Med 1992;28:275–289.

[39] Winkelmann S, Schaeffter T, Koehler T, Eggers H, Doessel O. An optimal radial profile order based on the golden ratio for timeresolved MRI. IEEE Trans Med Imaging 2007;26:68–76.

[40] Feng L, Grimm R, Block KT, et al. Golden-angle radial sparse parallel MRI: combination of compressed sensing, parallel imaging, and golden-angle radial sampling for fast and flexible dynamic volumetric MRI. Magn Reson Med 2014; 72:707-717. (The "GRASP" technique)

[41] Lebon V, Carlier PG, Brillault-Salvat C, Leroy-Willig A. Simultaneous measurement of perfusion and oxygenation changes using a multiple gradient-echo sequence: application to human muscle study. Magn Reson Imaging. 1998; 16:721–9.

[42] Duteil S, Wary C, Raynaud JS, Lebon V, Lesage D, Leroy-Willig A, Carlier PG. Influence of vascular filling and perfusion on BOLD contrast during reactive hyperemia in human skeletal muscle. Magn Reson Med. 2006; 55:450–4.

[43] Erin K Englund1, Michael C Langham1, Cheng Li1, Zachary B Rodgers1, Thomas F Floyd2, Emile R Mohler3 and Felix W Wehrli1. Combined measurement of perfusion, venous oxygen saturation, and skeletal muscle T2* during reactive hyperemia in the leg, Journal of Cardiovascular Magnetic Resonance 2013, 15:70.

[44] Wu W-C, Mohler E, Ratcliffe SJ, Wehrli FW, Detre JA, Floyd TF. Skeletal muscle microvascular flow in progressive peripheral artery disease: Assessment with continuous arterial spin-labeling perfusion magnetic resonance imaging. JACC 2009;53:2372–2377.

[45] Gr€ozinger G, Pohmann R, Schick F, et al. Perfusion measurements of the calf in patients with peripheral arterial occlusive disease before and after percutaneous transluminal angioplasty using MR arterial spin labeling. J Magn Reson Imaging 2013;40:980–987.

[46] Englund EK, Langham MC, Ratcliffe SJ, et al. Multiparametric assessment of vascular function in peripheral artery disease: dynamic measurement of skeletal muscle perfusion,

blood-oxygen-level dependent signal, and venous oxygen saturation. Circ Cardiovasc Imaging 2015;8:e002673–e002673.

[47] Anderson JD, Epstein FH, Meyer CH, et al. Multifactorial determinants of functional capacity in peripheral arterial disease: uncoupling of calf muscle perfusion and metabolism. JACC 2009;54:628–635.

[48] Elder CP, Cook RN, Wilkens KL, Chance MA, Sanchez OA, Damon BM. A method for detecting the temporal sequence of muscle activation during cycling using MRI. J Appl Physiol 2011;110:826–833.

[49] Jiji RS, Pollak AW, Epstein FH, et al. Reproducibility of rest and exercise stress contrast-enhanced calf perfusion magnetic resonance imaging in peripheral arterial disease. J Cardiovasc Magn Reson 2013;15:14.

[50] Duteil S, Wary C, Raynaud JS, et al. Influence of vascular filling and perfusion on BOLD contrast during reactive hyperemia in human skeletal muscle. Magn Reson Med 2006;55:450–454.

[51] T. C. Mamisch, T. Hughes, T. J. Mosher et al., T2 star relaxation times for assessment of articular cartilage at 3 T: a feasibility study, Skeletal Radiology, 2012; 41(3): 287–292.

[52] M. Barzin, M. Kowsarian, S. Akhlaghpoor, R. Jalalian, and M. Taremi, Correlation of cardiac MRI T2* with echocardiography in thalassemia major, European Review for Medical and Pharmacological Sciences, 2012; 16(2): 254–260.

[53] T. Kim, T. Murakami, M. Hori, H. Onishi, K. Tomoda, and H. Nakamura, Effect of superparamagnetic iron oxide on tumor-to-liver contrast at T2*-weighted gradient-echo MRI: comparison between 3.0 T and 1.5 T MR systems, Journal of Magnetic Resonance Imaging, 2009; 29(3): 595–600.

[54] A. N. Tong, X. Y. Lv, P. Yan, and Y. M. Wang, Magnetic resonance T2*-weighted study of U87 MG glioma tumors and its relationship between tumor hypoxia and VEGF expression, CNS Neuroscience and Therapeutics, 2013;19(3): 201–203.

[55] Lebon V, Carlier PG, Brillault-Salvat C, Leroy-Willig A. Simultaneous measurement of perfusion and oxygenation changes using a multiple gradient-echo sequence: application to human muscle study. Magn Reson Imaging. 1998; 16:721–9.

[56] Duteil S, Wary C, Raynaud JS, Lebon V, Lesage D, Leroy-Willig A, Carlier PG. Influence of vascular filling and perfusion on BOLD contrast during reactive hyperemia in human skeletal muscle. Magn Reson Med. 2006; 55:450–4.

[57] Erin K Englund, Michael C Langham, Cheng Li, Zachary B Rodgers, Thomas F Floyd, Emile R Mohler and Felix W Wehrli. Combined measurement of perfusion, venous oxygen saturation, and skeletal muscle T2* during reactive hyperemia in the leg, Journal of Cardiovascular Magnetic Resonance 2013, 15:70.

[58] Dana C. Peters, J. Andrew Derbyshire, and Elliot R. McVeigh. Centering the Projection Reconstruction Trajectory: Reducing Gradient Delay Errors. Magn Reson Med. 2003 Jul; 50(1): 1–6.

[59] Block K, Uecker M. Simple method for adaptive gradient-delay compensation in radial MRI. In Proceedings of the 19th Annual Meeting of ISMRM, Quebec, Canada, 2011. p. 2816.

[60] Tess Armstrong , Isabel Dregely , Alto Stemmer, Fei Han, Yutaka Natsuaki, Kyunghyun Sung and Holden H. Wu. Free-Breathing Liver Fat Quantification Using a Multiecho 3D Stack-of-Radial Technique. Magn Reson Med. 2017; 00:00–00 .

[61] Raynaud JS, Duteil S, Vaughan JT, Hennel F, Wary C, Leroy-Willig A, Carlier PG. Determination of skeletal muscle perfusion using arterial spin labeling NMRI: validation by comparison with venous occlusion plethysmography. Magn Reson Med. 2001; 46:305–11.

[62] Erin K Englund, Zachary B Rodgers, Michael C Langham, Emile R Mohler III, Thomas Floyd, and Felix W Wehrli, Simultaneous measurement of macro- and microvascular blood flow and oxygen saturation for quantification of muscle oxygen consumption; Magn Reson Med. 2018 February ; 79(2): 846–855.

[63] Kiril Schewzow, Georg Bernd Fiedler, Martin Meyerspeer, Sigrun Goluch, Elmar Laistler, Michael Wolzt, Ewald Moser, and Albrecht Ingo Schmid, Dynamic ASL and T2*-Weighted MRI in Exercising Calf Muscle at 7 T—A Feasibility Study , Magn Reson Med, 2015; 73:1190–1195.

[64] Rooney WD, Johnson G, Li X, et al. Magnetic field and tissue depend-encies of human brain longitudinal 1H2O relaxation in vivo. MagnReson Med 2007;57:308–318.

[65] Calamante F, Thomas DL, Pell GS, Wiersma J, Turner R. Measuring cerebral blood flow using magnetic resonance imaging techniques. JCerebr Blood F Met 1999;19:701–735.

[66] X. Zhang, E. T. Petersen, E. Ghariq, J. B. De Vis, A. G. Webb, W. M. Teeuwisse, J. Hendrikse, and M. J. P. van Osch, In Vivo Blood T1 Measurements at 1.5 T, 3 T, and 7 T, Magn Reson Med 70:1082–1086, 2013.

[67] Raynaud JS, Duteil S, Vaughan JT, Hennel F, Wary C, Leroy-Willig A, Carlier PG. Determination of skeletal muscle perfusion using arterial spin labeling NMRI: validation by comparison with venous occlusion plethysmography. Magn Reson Med. 2001; 46:305–11.

[68] Erin K Englund, Michael C Langham, Cheng Li1, Zachary B Rodgers, Thomas F Floyd, Emile R Mohler and Felix W Wehrli1. Combined measurement of perfusion, venous oxygen saturation, and skeletal muscle T2* during reactive hyperemia in the leg, Journal of Cardiovascular Magnetic Resonance 2013, 15:70.

[69] Kiril Schewzow, Georg Bernd Fiedler, Martin Meyerspeer, Sigrun Goluch, Elmar Laistler, Michael Wolzt, Ewald Moser, and Albrecht Ingo Schmid, Dynamic ASL and T2*-Weighted MRI in Exercising Calf Muscle at 7 T—A Feasibility Study , Magn Reson Med, 2015; 73:1190–1195.

[70] Erin K Englund, Zachary B Rodgers, Michael C Langham, Emile R Mohler III, Thomas F Floyd, and Felix W Wehrli, Simultaneous measurement of macro- and microvascular blood flow and oxygen saturation for quantification of muscle oxygen consumption; Magn Reson Med. 2018; 79(2): 846–855.